LASER SPECKLE IMAGING: A QUANTITATIVE TOOL FOR FLOW ANALYSIS

A Thesis

presented to

the Faculty of California Polytechnic State University,

San Luis Obispo

In Partial Fulfillment

of the Requirements for the Degree

Master of Science in Biomedical Engineering

by

Taylor Andrew Hinsdale

June 2014

© 2014
Taylor Andrew Hinsdale
ALL RIGHTS RESERVED

COMMITTEE MEMBERSHIP

TITLE:	Laser Speckle Imaging: A Quantitative Tool for Flow Analysis
AUTHOR:	Taylor Andrew Hinsdale
DATE SUBMITTED:	June 2104
COMMITTEE CHAIR:	Lily Laiho, PhD Associate Professor of Biomedical Engineering
COMMITTEE MEMBER:	David Clague, PhD Associate Professor of Biomedical Engineering
COMMITTEE MEMBER:	John Sharpe, PhD Professor of Physics

ABSTRACT

Laser Speckle Imaging: A Quantitative Tool for Flow Analysis
Taylor Andrew Hinsdale

Laser speckle imaging, often referred to as laser speckle contrast analysis (LASCA), has been sought after as a quasi-real-time, full-field, flow visualization method. It has been proven to be a valid and reliable qualitative method, but there has yet to be any definitive consensus on its ability to be used as a quantitative tool. The biggest impediment to the process of quantifying speckle measurements is the introduction of additional non dynamic speckle patterns from the surroundings. The dynamic speckle pattern under investigation is often obscured by noise caused by background static speckle patterns. One proposed solution to this problem is known as dynamic laser speckle imaging (dLSI). dLSI attempts to isolate the dynamic speckle signal from the previously mentioned background and provide a consistent dynamic measurement. This paper will investigate the use of this method over a range of experimental and simulated conditions. While it is believable that dLSI could be used quantitatively, there were inconsistencies that arose during analysis. Simulated data showed that if the mixed dynamic and static speckle patterns were modeled as the sum of two independent speckle patterns, increasing static contributions led to decreasing dynamic contrast contributions, something not expected by theory. Experimentation also showed that there were scenarios where scattering from the dynamic media obscured scattering from the static medium, resulting in poor estimates of the velocities causing the dynamic scattering. In light of these observations, steps were proposed and outlined to further investigate into this method. With more research it should be possible to create a set of conditions where dLSI is known be accurate and quantitative.

ACKNOWLEDGMENTS

During my time at Cal Poly there has been several influential and supportive figures in my life. I cannot begin to name all of them, but I would like to take this opportunity to acknowledge those who helped me immensely during my thesis. Firstly, I would like to acknowledge my advisor Dr. Lily Laiho for guiding me through this project. Her mentoring throughout my last years here and during this project was invaluable. I would also like to thanks Dr. John Sharpe for advising me on much of the optical theory relating to this project. Another huge help was Chad Nelson from Coherent. He was able to help me acquire the Laser necessary to undertake this task and I could not have done or afforded it as easily without him. Dr. Richard Savage also aided in my acquisition of the optical components necessary for this project, and for that I am truly grateful. I would also like to acknowledge Dr. Pavel Zhakarov for his contribution of the dLSI code, and Dr. Donald Duncan and Dr. Sean Kirkpatrick for their contributions to the speckle simulation code. To my mother, father, sister, family and friends who are too many to name, your support and friendship during my college years was irreplaceable. You have helped get me this far and I hope will continue to do so.

TABLE OF CONTENTS

LIST OF TABLES

LIST OF FIGURES

Chapter 1: Introduction

1.1 Laser Speckle Imaging Overview

The desire for non-invasive, real time, and accurate fluid velocity measurement in medical research and diagnostics has driven the research in laser based methods. One current technique being employed is laser Doppler flowmetry, which is based on the interference caused by light scattering objects that are under motion. Problems arose with this method when measurements could only be made at a single point in space, requiring mechanical scanning for full field imaging. This undesirable quality led to the development of a technique known as laser speckle contrast analysis (LASCA). Real time velocity measurements and blood perfusion measurements could now be made over a larger field of view. Many researchers have applied this; with some demonstrating the effectiveness of LASCA, also known as laser speckle imaging, for characterizing real time blood perfusion in patients who underwent treatment for port wine stain. [1] Others have applied the method in areas such as microvasculature flow assessment and atherosclerotic plaque characterization, but up until recently most efforts have been qualitative rather than quantitative in nature. [3][4][5][17]

1.2 Fundamentals of LASCA

The laser speckle phenomenon arises from coherent light incident upon a scattering medium. The easiest way to represent a scattering medium is an uneven planar surface. Figure 1 below shows in a diagram how the interference occurs and gives an example of a typical speckle pattern.

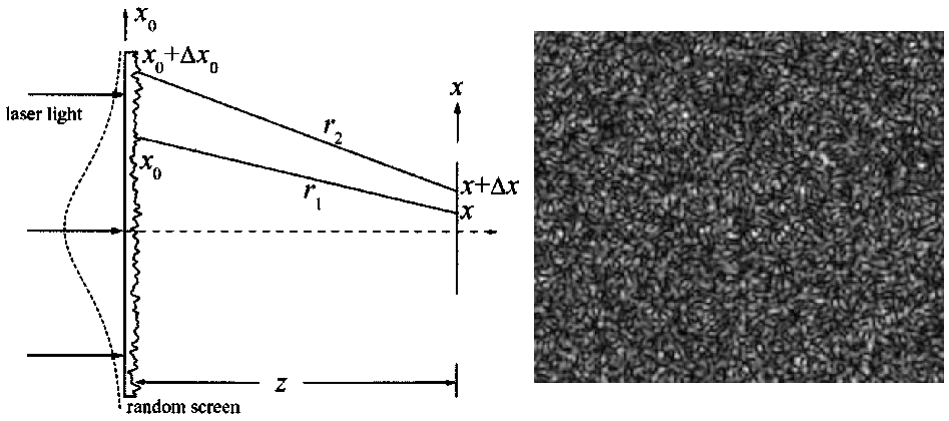

Figure 1 – Speckle formation example. (Left) Illumination of uneven surface by coherent light source producing a speckle pattern at the imaging plane. (Right) Characteristic speckle pattern that arises from the process on the left. [24][14]

Light incident upon this surface will reflect; however, since the light has now traveled different path lengths due to the uneven plane heights, it will interfere. The observer will see the summation of many scattered light waves and their interference pattern. Because the unevenness of the plane is essentially random, the interference pattern of the light is random and will create a distribution of light and dark spots.

The laser speckle phenomena can be used to extract information from the illuminated surface that produces the pattern. The standard measure of a speckle pattern is known as the contrast, which is shown below in Equation 1.

(1) $$K = \frac{\sigma_s}{<I>}$$

The contrast is a measure of the variation in the intensity of the speckle pattern and, as seen in Equation 1, is defined as the ratio of spatial standard deviation, σ_s, to the mean intensity, <I>, of the speckle pattern. If the speckle pattern is formed from light scattering

off a dynamic medium, the variable of contrast can be utilized to infer information about velocity of the dynamic medium.

A paper published by Fercher and Briers in 1981 derived a relationship that could be used to relate moving speckle patterns to velocities using single exposure photography. [11] Advances in technology have changed the way speckle images are captured, but the principles they laid out still apply and act as the foundation of laser speckle contrast analysis. For the purposes of blood flow analysis, LASCA analyzes the temporal and spatial fluctuations in a speckle pattern. It assumes that regions of speckle caused by a static background will remain static and regions caused by a dynamic background will change over time. The simplest formulation of LASCA relates the spatial standard deviation of the speckle intensity, σ_s, divided by the mean speckle intensity, <I>, to speckle field autocorrelation function, $g_1(\tau)$. The decorrelation time, τ_c, and camera exposure time, T, are parameters of the autocorrelation function. [11]

$$\frac{\sigma_s}{<I>} = \frac{1}{T}\int_0^T |g_1^2(\tau)|d\tau = \left[\left(\frac{\tau_c}{2T}\right)\left\{1 - \exp\left(\frac{-2T}{\tau_c}\right)\right\}\right]^{1/2} \quad (2)$$

Relating this to what is physically observed, the spatial standard deviation is a measure of the blur caused by speckles under motion. This occurs due to a finite exposure time, which creates a temporal averaging effect when speckles are in motion.
The left hand side of Equation 2 are the measured variables in LASCA. The right hand side is the information we wish to infer. The middle is time integral of the speckle autocorrelation function, which will be discussed shortly. The measured values for Equation 1 are the raw image intensity. The raw intensity information is then processed

to display the spatial standard deviation divided by the mean intensity of the image. The quantity used to represent the standard deviation of the speckle intensity by the mean intensity is the contrast, K, as shown in Equation 1. [11]

Equations 2 is a statistical approach to characterizing dynamic speckle behavior. The contrast in Equation 2 is bounded by the values zero and one. A value of zero occurs when the standard deviation of the speckle intensity pattern is zero. This physically makes sense when imaging on a camera with a finite exposure time; fast enough speckles will cause a blurring effect and homogenize the resulting image causing a contrast of zero as the standard deviation of the intensity approaches zero. A value of one occurs when the standard deviation of the speckle intensity pattern is equal to the mean intensity of the speckle pattern. Both of these are fundamental features speckle and are the resultant of the mathematical upper and lower bounds for contrast.

A key concept to keep in mind is that the spatial variance of a speckle pattern is related to the time averaged autocorrelation of the speckle pattern as seen in Equation 2. [13] The autocorrelation function represents a function's, or pattern's, self-similarity. In our case we are considering the time evolution of a signal. The autocorrelation procedure takes the time evolving signal at one point in time and compares it with a time evolved version of itself. This procedure produces what is known as the autocorrelation function. The autocorrelation function starts with a value of one on the y-axis and decays as it moves along the x-axis, which is in units of time, in the positive direction. How fast this function decays to zero is a measure of how dissimilar the time varying signal has become. This decay time is known as the decorrelation time and translates to how fast the signal is time evolving. For laser speckle, two speckle patterns that are identical are

perfectly correlated, while two speckle patterns that are statistically independent are completely uncorrelated. [13] The autocorrelation function measures how fast the transition between these two states is occurring in a dynamic speckle pattern. Since the autocorrelation function cannot be measured instantaneously with current methods, it must be time averaged. The time average of this autocorrelation function can be related to the spatial statistical properties of the dynamic speckle pattern, and this is what is shown in Equation 2. [13] This translates physically to the signal that a CCD camera acquires with a set exposure time. Measuring the contrast of a dynamic pattern as seen by the CCD then allows for the interpolation of the ratio $\frac{\tau_c}{T}$ through Equation 2. Knowing the exposure time of the system then allows for an estimate of the decorrelation time. Using this basic approach one can make a qualitative assessment of flow rates in a system. If a quantitative analysis of the system flow is desired, modifications need to be made to the LASCA algorithm.

1.3 Quantitative Dynamic (dLSI) Method

An approach known as dynamic laser speckle imaging has been used to conduct quantitative laser speckle flow analysis in the presence of background scatterers, with background scatters being defined as a static component that contributes unvarying speckle to the dynamic pattern. [27] An example of background scatters in blood flow imaging is the vessel wall and background tissue surrounding the flowing blood. These components scatter light that interferes with the dynamic speckle pattern formed by the blood. This method falls largely from the work of Zhakarov et al. [27] In this model static scattering components of the speckle image are assumed mixed with the dynamic

scattering parts. [27] The fluctuations in a coherently scattered field, $g_1(\tau)$, as shown in Equation 3, can be described by the autocorrelation function of the speckle field which is approximated by a negative exponential as discussed earlier. [27]

(3) $$g_1(\tau) = \exp(-\delta\tau^n)$$

δ and n depend on the exact model being used to describe the scattering light. Reference Zhakarov et al. [27] for more information regarding the model of diffusing wave spectroscopy (DWS) that they used and the resulting δ and n. In order to relate this to a measurable value, the Siegert relation is employed, shown in Equation 4. It relates the electric field autocorrelation function $g_1(\tau)$ to the intensity field autocorrelation function $g_2(\tau)$.[27] Note that the following relationship is only true if the field obeys Gaussian random statistics.

(4) $$g_2(\tau) = 1 + \beta|g_1(\tau)|^2$$

β is coherence factor that describes the amount of contributing speckles being recorded by a given camera pixel. [27] Now that the static and dynamic contributions are being accounted for, $g_1(\tau)$ is modified with the value $g_{1d}(\tau)$ and ρ. $g_{1d}(\tau)$ is the measured static and dynamic contributions; ρ is used to represent just the static contribution to the function. [27]

(5) $$g_1(\tau) = (1-\rho)|g_{1d}(\tau)| + \rho$$

Combining Equations 4 and 5 produces the intensity autocorrelation function of a statically and dynamically mixed intensity signal (Equation 6).

(6) $$g_2(\tau) = 1 + \beta[|(1-\rho)g_{1d}(\tau)| + \rho]^2$$

Substituting Equation 6 into the modified version of Equation 1 yields Equation 7. K_{1d} represents the mixed contrast of the electric field and K_{2d} the mixed contrast of the intensity. [27]

(7) $$K_m^2 = \left(\frac{2\beta}{T}\right)\int_0^T [(1-\rho)|g_{1d}(\tau)| + \rho]^2\left(1 - \frac{\tau}{T}\right) d\tau$$

$$K_m^2 - \beta\rho^2 = K_{12d}^2 = (1-\rho)^2 K_{2d}^2 + 2\rho(1-\rho)K_{1d}^2$$

Ideally, ρ is equal to zero and K_m reduces to K_{2d}; however ρ is usually greater than 0. Evaluating the expression in Equation 7 is difficult and impractical. [27] The method suggested for circumventing this problem is to estimate the static contribution to the intensity by cross correlating two images that were taken of the same flow pattern. [27] However, certain assumptions need to be made to make use of this method. It is necessary to assume that there is no correlation between the dynamic speckle patterns within successive frames during multiple exposures, i.e. multiple images. [27] For this to be true, the relation $\Delta t > T \gg \tau_c$, where Δt is the time between frames, T is the exposure time, and τ_c is the intensity decorrelation time. [27] The following expression (Equation 8) for the static component exists if we take from the assumptions above that

$g_{1d}(\tau)$, which is the dynamic autocorrelation function, equals zero on a time scale of Δt. [27]

(8) $$\rho^2 = [g_2(\Delta t) - 1]/\beta$$

What this says is that if subsequent images are cross correlated under the assumption that the cross correlation between the dynamic patterns is zero, the only contribution to the cross correlation will be from the static pattern. See Appendix A for a flowchart describing the process.

Relating the decorrelation times calculated using the equations above to velocity has proven to be rather difficult. Some propose the decorrelation velocity v_c is related to the wavelength, λ, and the decorrelation time, τ_c, shown in Equation 9 below. [8]

(9) $$v_c = \frac{\lambda}{2\pi\tau_c}$$

This equation is largely an educated guess and other theories will be explored in the discussion section of this paper.

1.4 Speckle Simulation

Speckle can be thought to exist in two modes, objective and subjective. [8] An objective speckle pattern exists in an observation plane as a result of scattered light from a surface. It is unaltered by imaging optics with the size being linearly related to the diameter of the illuminating coherent source, the wavelength of that source, and the

distance that the observation plane is away. [8] The speckles grow as the observation plane retreats from the source. [8] Each speckle behaves much like an airy pattern seen in circular diffraction, spreading out over space.

The objective speckle field can be modeled by populating an array with randomly distributed complex numbers of magnitude unity. [8] Magnitude unity ensures equal contribution from all frequency components. Randomizing the phases simulates the random phase shifts that coherent light undergoes after scattering off a rough surface. Creating a circular mask, which represent the diameter of the coherent source, in the array and Fourier transforming the elements inside the mask with those outside equal to zero yields a fully developed speckle pattern. [8] This is due to relation between spatial frequency and space in Fourier analysis. The spread of features in the spatial dimension is inversely proportional to the spread of features in the spatial frequency realm. Controlling the ratio of the diameter of the mask to the length of the array controls the speckle size. [8] When the diameter is half the length of the length of the array, the minimum speckle size is 2 pixels, and will satisfying the Nyquist criterion for spatial speckle sampling. [8]

Understanding objective speckle is required to build a strong foundation regarding speckle simulation; however, a much more realistic scenario is the case of subjective speckle. Subjective speckle is the observed speckle pattern created by scattering off of a surface as it appears in the imaging plane of an imaging system. [8] The idea of the circular mask must be now be reinterpreted; the aperture is now physically considered to be the emitting source of light. Instead of representing the diameter of the coherent source, the circular mask now represents the diameter of the aperture of the imaging system. [8]

Simulating movement requires that the phase pattern is translated through the pupil, which is simulated by translating the mask through the complex array. [8] This creates a speckle pattern that transforms into another and becomes completely uncorrelated when the mask has shifted the length of its diameter in the array. A lack of translational movement in the imaging plane will occur and is a result geometric optics. [8] This phenomenon is known as speckle boiling and is illustrated in Figure 2 below. [8]

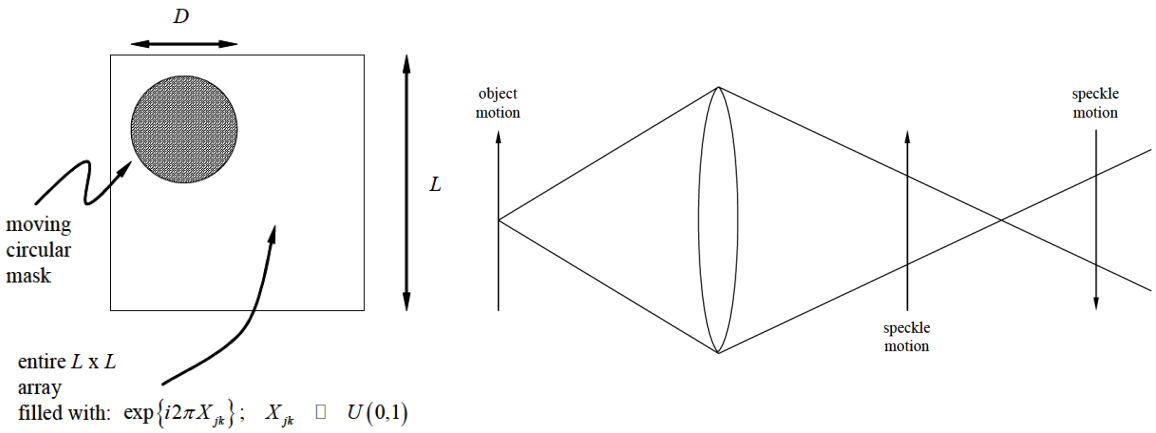

Figure 2 – Simulated speckle illustration. (Left) Illustration of the movement showing the circular aperture moving through the complex plane. (Right) Object motion represent in the focal plane. The image moves with the object motion in front of the image and opposite the motion behind it, with the boiling phenomena occurring precisely at the image plane. [8]

Speckle in front of the image plane tracks with the speckle in the object plane while speckle behind the image plane tracks in the opposite direction. The transition in these directions occurs at the focus and is a result of geometric optics. [8] In reality, imaged speckle is never entirely at the focus. Some out of focus speckle will contribute to the image. This would call the for superposition of translational as well as boiling speckle in simulation, but for this experiment boiling will be sufficient for preliminary investigation.

Chapter 2: Methods and Materials

2.1 Methods Overview

The LASCA experimental procedure consists of a few basic elements. The necessary essentials are a coherent light source, i.e. laser, the imaged object, and a CCD camera used to capture the images as shown in Figure 3.

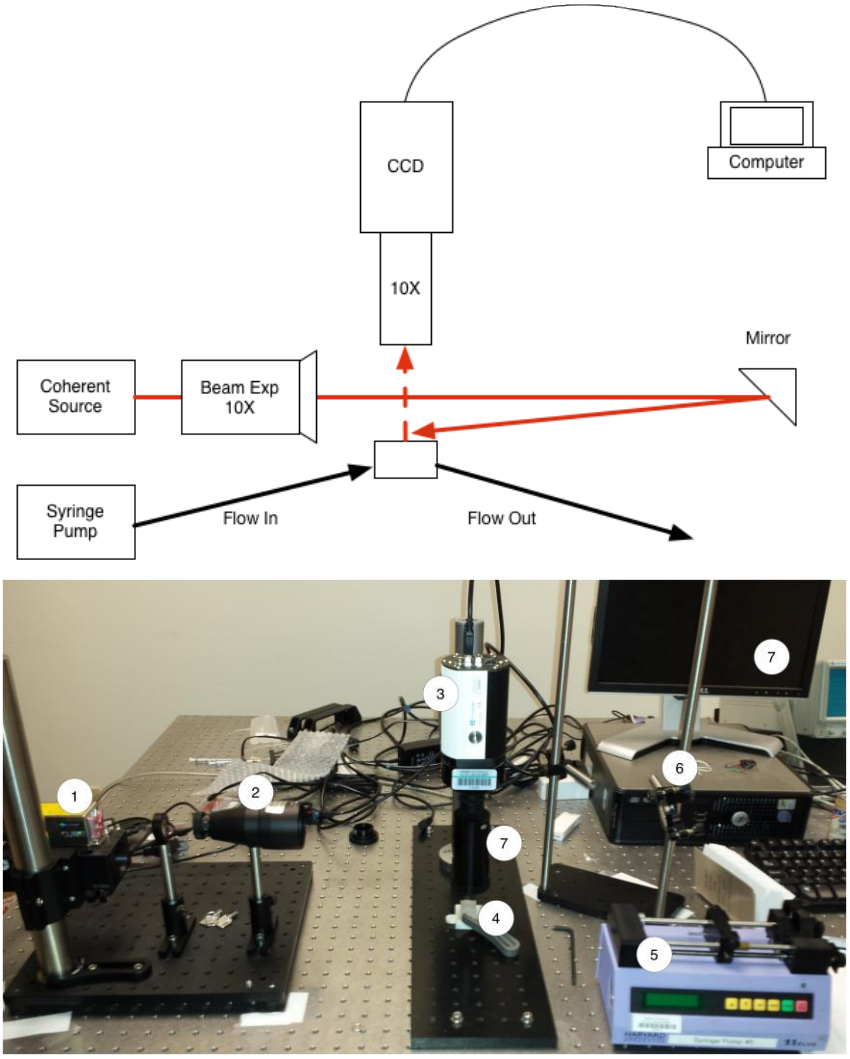

Figure 3 – Laser speckle contrast analysis experimental imaging construct. (Top) A coherent beam is steered onto the tissue phantom, which is then imaged by a CCD camera with a 10X macro zoom lens. The image acquired is approximately 8x8 mm^2. (Bottom) Experimental Setup: (1) Coherent Cube laser (2) ThorLabs beam expander (3) Retiga CCD (4) Tissue phantom (5) Harvard Apparatus syringe pump (6) Turning mirror (7) Image acquisition computer

As well as providing a diagram of a typical LASCA setup, Figure 3 also shows the specific configuration that was used in image acquisition for this project. One of the primary benefits of LASCA is noted in the simplicity of its set up. The configuration used for this experiment consisted of a coherent light source, beam expanding optics, a steering mirror to direct the light where it is needed, a tissue phantom and accompanying syringe pump to create fluid flow over it, and a CCD camera with imaging optics. Standard software, such as QCapture Image Suite, is used to capture images of the dynamic speckle pattern. An algorithm is then used to compute the contrast values and decorrelation times of the speckle images captured by the CCD camera. The following sections provide a more detailed look at the equipment used and the methods implemented.

2.2 CCD Camera

A Retiga 2000R (Retiga-2000R Fast 1394 Mono Cooled Model: RET-2000R-F-M-12-C) CCD camera was used for image acquisition. A 10X Computar macro zoom lens (MLH-10X 1/2" 13 to 130mm 10x Close-up Manual Zoom/Iris Lens C-Mount) was attached to the CCD camera in order to obtain the appropriate field of view. An extension tube kit (Computar VM100) was also used in conjunction with the macro zoom lens in order to bring working distance of the camera closer to the lens, allowing the CCD to focus closer to the micro capillary tissue phantom.

2.3 Laser and Optical Components

A Coherent Cube (CUBE 640-40C) 640 nm 40 mW laser diode served as the coherent source for this experiment. A ThorLabs 10X beam expander (BE10M-A) was used in conjunction with a ThorLabs NBK-7 30mm focal length lens (LA1289-A) to create a roughly 10mm diameter beam size. A silvered mirror attached to an adjustable mount was used to guide the beam to its final destination.

2.4 Tissue Phantom and Flow Apparatus

The primary goal of the tissue phantom was to replicate the background scattering of biological tissue; this was done by using a polymeric material (PDMS) that was infused with scattering agents until it was optically similar to biological tissue. [15] The tissue phantom was also designed to stably hold capillary tubes superficially with fluid flow in order to simulate blood flow over a biological medium. In order to create geometry suitable for both of these purposes, a mold was made in SolidWorks. The mold created a phantom that was flat on top, providing a surface for the capillary tube to rest upon. Figure 4 below shows a typical tissue phantom used in this project and the mold used to create them.

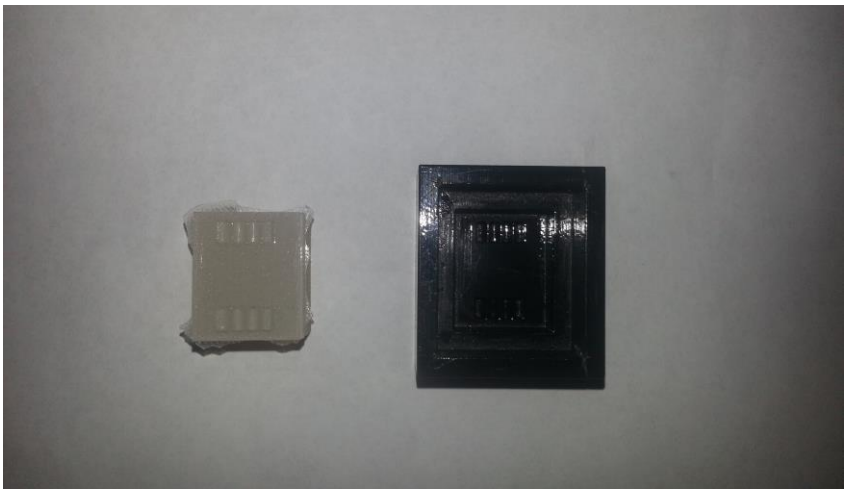

Figure 4– Tissue phantom and mold example. The tissue phantom on the left contains of a concentration of 1 mg/mL of TiO_2/PDMS. The mold on the right is a negative of the features.

Additionally, there were small protrusions on the top of the phantom, which would hold the press-fitted capillary tube in place. The mold was made using a stereolithography 3D printer with tolerances of 4 microns.

184 Sylgard PDMS gel (Dow Corning, Midland, MI) was selected as the phantom material due to its optical properties, as it exhibits a similar index of refraction (approx. 1.4) to that of human tissue. [15] Additionally, titanium dioxide nano-particles (677469, Sigma Aldrich, St. Louis, MO), scattering agents, were mixed in with the uncured PDMS gel at concentrations of 0 mg/ml, 0.5 mg/ml, 1 mg/ml, and 2 mg/ml. The mixture was then subjected to sonication to evenly disperse them throughout the mixture. The mixture was then poured into the mold and run through a vacuum chamber to reduce the formation of air bubbles. While in the vacuum chamber the pressure was reduced to allow air bubbles in the PDMS to rise to the top of the mold. Once the surface of the PDMS was populated with bubbles, the pressure was returned to atmospheric, thus

popping the bubbles. This process was repeated until the formation of air bubbles ceased. The phantom was then allowed to cure for 48 hours before removing it from the mold.

A capillary tube (282 μm, Drummond Microcap, P1799 Sigma Aldrich, St. Louis, MO) was then press fit into place, resting atop the phantom and in direct contact with the surface. Tygon tubing was connected to the capillary tube and a syringe pump (Harvard Apparatus, Holliston, MA). Full fat vitamin D milk (Crystal Milk, Modesto, CA) was pumped through at constant rates of 5, 10, 15, 20, and 25 μL/min, simulating the range of blood flows found in vasculature. Milk was chosen as a substitute for blood due to it being a blood derivative and easily obtainable. Fats and proteins in the milk exhibit similar scattering properties to those found in blood.

2.5 dLSI: Simulated Speckle

To test this method under ideal conditions, a simulated dynamic speckle pattern was constructed. As stated before, the contrast of a laser speckle image, which was defined in equation 1 and 2, is the ratio of the spatial standard deviation to the average intensity of the laser speckle image. In practice, LASCA is a simplistic method for analyzing qualitative changes in flow, but this paper attempts to investigate quantitative methods. To do this dynamic laser speckle imaging was utilized. This involves assuming that the acquired signal is mix of static and dynamic speckle patterns. The static part is estimated using a time series correlation technique and subtracted from the mixed signal. The resultant is the purely dynamic part of the signal.

Using the translational aperture method, the data acquisition of a dynamic speckle pattern by a CCD camera could be mimicked. The dynamic contrast is related to a

function of τ_c/T. Knowing that the decorrelation time τ_c is reached when the aperture has translated one full diameter allows for the creation of time averaged images for varying ratios of τ_c/T. For example, in this experiment the aperture is 252 pixels in diameter, with a full decorrelation taking 253 frames while translating at 1 pixel per shift. For a ratio of τ_c/T = 1 all 253 frames must be averaged together. To get a ratio of τ_c/T < 1 the series needs to be averaged over more than 253 frames. It is important to note that when extending the frames a new statistically independent speckle pattern should be generated and concatenated to preserve the assumptions of the dLSI method.

An acquisition series of 30 "exposures" is then created to simulate the multiple exposure averaging used in the dLSI method; once again it is important to have statistically independent speckle patterns. A set of 30 images was chosen to ensure that the maximal contrast of the condition being imaged was obtained through a temporal averaging technique which dLSI utilizes. [7] This is critical between "exposures" so that the correct static contribution can be estimated. Using fewer images may underestimate the contrast. [7] The static contribution was introduced by imposing an unvarying pattern on all images in the series. Its intensity relative to the dynamic pattern was varied to simulate varying contributions from static scattering. This was accomplished by creating a static pattern with the same average intensity as the dynamic pattern and multiplying it by a scalar to either make it more intense or less intense relative to the dynamic pattern.

Once the series images were constructed, the data set is analyzed using the dLSI method. This provided estimations of the static contribution to the pattern, the dynamic contribution, and the decorrelation time. This was done for the ratios τ_c/T: 0.02, 0.06,

0.08, 0.1, 0.2, 0.5, 0.8, and 1. Each ratio contained a series of 30 images with independent dynamic speckle patterns.

2.6 dLSI: Experimental Data

Milk was pumped at a rate of 250 μL/min through the flow apparatus until the tubing was filled solely with milk. Once again milk was chosen due to it having distribution of colloidal particles between 0.1 – 1 um, approximately similar to blood, and its availability. [16] While blood cells typically range on a size scale of ~6 um in diameter, it was decided that milk would suffice and the difference in colloidal particle size would be negligible. The syringe pump was then stopped, allowing the fluid to come to rest. Then the fluid could be pumped through a series the desired flow rates (1, 3, 5, 10, 15, 20, or 25 μL/min). Once a constant flow was established for a given flow rate, a series of images of the capillary was taken (30 images, 5ms exposure time on the CCD camera, with a 5ms or greater interval between captures to satisfy the criteria for the static estimation). In order to clean the apparatus for the next sample, the tubing setup was initially flushed with 5 mL of distilled water and then with air. The syringe was also flushed repeatedly with distilled water to prevent contamination between samples. The data sets were then immediately ready for processing with the dynamic speckle algorithms.

Chapter 3: Results

3.1 Results Overview

After implementing the dLSI method on both the simulated speckle images and experimental speckle images, the results needed to be examined to determine if a consistent relationship between the static contribution and the dynamic contrast could be established and whether or not dLSI could accurately predict velocities during experimentation. The simulated data provided insight into the behavior of the function relating contrast to decorrelation times, while the experimental data showed that there are physical limitations of the method.

Different models of the autocorrelation function can be used to relate the dynamic contrast to the decorrelation time in the dLSI method. The form of the autocorrelation function primarily depends on the characteristics of the flow pattern being investigated. Initially only the diffusing wave spectroscopy (DWS) model of the autocorrelation function was to be implemented; this was the original model that the originators of the dLSI method proposed. It was soon realized that there were deviations between the measured data from the simulation and the theoretical values that were predicted by the DWS model. In order to account for this, the DWS autocorrelation model for relating decorrelation time to contrast was reformulated into its most basic form, the Lorentzian flow model of the speckle field autocorrelation function. [2] An empirical adjustment function was then introduced to the Lorentzian flow model to force it to behave like the simulated data. To clarify, the dLSI method for estimating the dynamic contrast and decorrelation times was implemented using two different models of the autocorrelation function, DWS and empirical.

The four different aspects investigated were: the dSLI analysis of the dynamic laser speckle simulation using the diffusing wave spectroscopy (DWS) model, the dLSI analysis of the experimental data using the DWS model, the dLSI analysis of the dynamic laser speckle simulation using the empirical model, the dLSI analysis of the experimental data using the empirical model, and the statistical scattering distributions of the experimental data.

3.2 Simulation Results

Simulation was undertaken in order to better understand the behavior of the dLSI method because simulated parameters are much easier to control than experimental parameters.

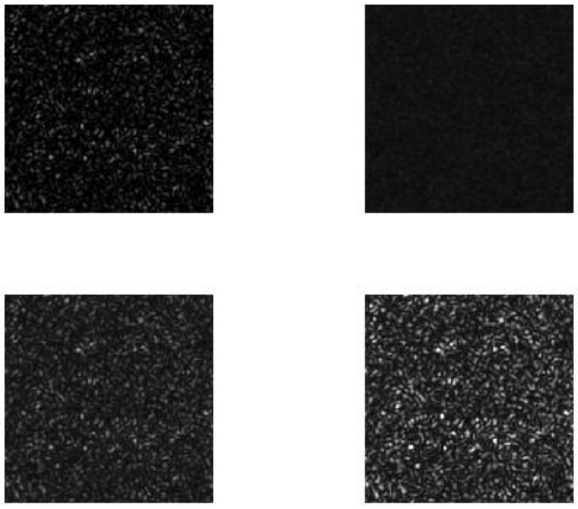

Figure 5– Representative simulated speckle patterns. (Top Left) Static speckle pattern (Top Right) Dynamic speckle pattern without added static pattern (Bottom Left) Dynamic and static speckle superposition of equal intensity (Bottom Right) Dynamic and static speckle superposition with static intensity 2X. All dynamic patterns were generated with a $\tau_c/T = 0.08$.

Simplifying the dynamic and static speckle superposition to ideal conditions allowed for the analysis of the dLSI method without external sources of error. Figure 5 is representative of typical speckle patterns generated during simulation. Each pattern in Figure 5 is considering only a $\tau_c/T = 0.08$, see the appendix for more examples. As expected, the pattern with no static contribution is very uniform but is overcome by the static pattern as its relative intensity is increased.

3.2.1 DWS Simulation

An interesting phenomenon emerged from the simulated experiment that needs to be addressed. When calculating the theoretical decorrelation time, given a calculated dynamic contrast and static contribution to the pattern, there appears to be a significant

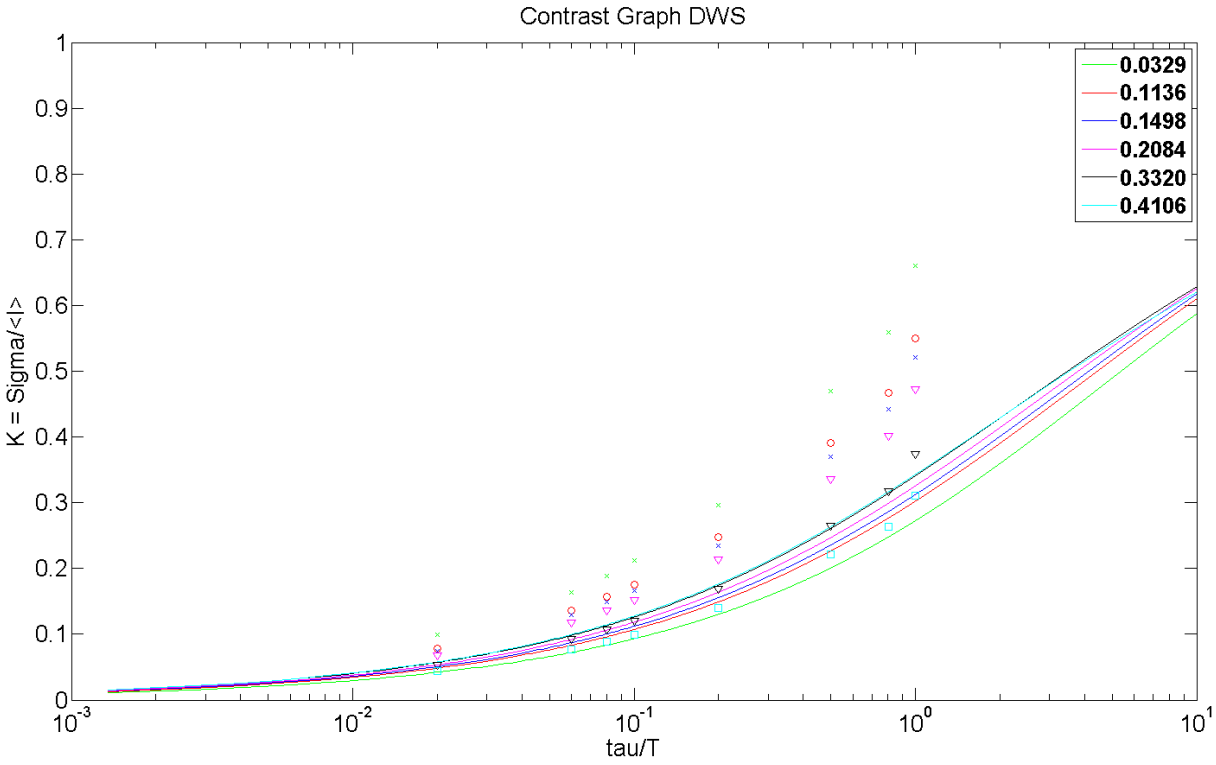

Figure 6 – Ratio of decorrelation time divided by exposure time graphed against dynamic contrast using the DWS scattering model. Legend contains the estimated static contrast contribution. Plotted points are the simulated data and the plotted lines are the theoretical values.

divergence between theory and simulated experiment. Figure 6 shows that given a dynamic contrast, not only are the decorrelation values over estimated by theory, but they also exhibit the opposite trend suggested by simulation. The trend is referring to the simulation giving a decreasing dynamic contrast as the static contribution increases for a given decorrelation time. The data represented by the points in Figure 6 are the calculated dynamic contrast for the simulated speckle images. The lines represent the theoretical relationship between dynamic contrast and the decorrelation time for the DWS autocorrelation model. The color code in the legend represents differing values of static contrast contribution.

Table 1 shows the percent errors between the simulated data and the values predicted by theory. The rows correspond to different values of estimated static scattering and the columns refer to varying ratios of τ_c/T. Table 1 helps gives a numerical representation of the differences between the simulated data and the theoretical predictions of the DWS autocorrelation model.

Table 1: Percent error between simulated experiment and theory for DWS model

	Percent Error (Exp – Theory)/Exp*100							
	τ_c/T							
$\boldsymbol{\rho}$	**0.02**	**0.06**	**0.08**	**0.1**	**0.2**	**0.5**	**0.8**	**1**
0.0329	75.91	44.269	38.222	34.552	26.187	15.105	11.576	5.0744
0.117	22.386	13.42	11.497	10.665	9.1365	4.6804	3.7728	-1.3678
0.1498	30.943	18.358	15.726	14.429	11.757	6.4679	5.0856	0.19284
0.2084	62.58	36.394	31.454	28.423	21.457	12.78	9.7582	5.0896
0.332	40.031	23.415	20.865	18.289	14.158	7.8962	6.3092	2.6171
0.4106	-271.7	-142.3	-122.3	-110.3	-76.30	-49.14	-36.17	-37.155

3.2.2 Lorentzian Flow Analysis of the Simulation

The DWS autocorrelation model in Figure 6 is set up to account for the specific scattering characteristics of blood and similar biological media. However, the simulation was run under the assumption that the particles are not in Brownian but are undergoing linear flow, essentially operating under the Lorentzian flow assumptions; this means differences between the simulated data and the theoretical predictions for the DWS model were to be expected. Noting the large percent differences in Table 1, a rederivation of the autocorrelation function in Equation 3 was made. To simplify the problem, δ was made equal to $1/\tau_c$, where τ_c is the characteristic decorrelation time, and n was set equal to 1. This creates a function that assumes a Lorentzian flow distribution, i.e a single scattering non-diffusion driven case, which is what Equation 2 was formulated under the assumption of. A plot of this was made and is shown in Figure 7. The simulated data points are the same as the simulated data points in Figure 6. The only difference is that the relationship between the dynamic contrast and the decorrelation time has changed. This can be seen in the shifting of the theoretical lines upward. Table 2 shows the resultant error with this new simplified model. It contains the same information as Table 1 but draws from data obtained from Figure 7.

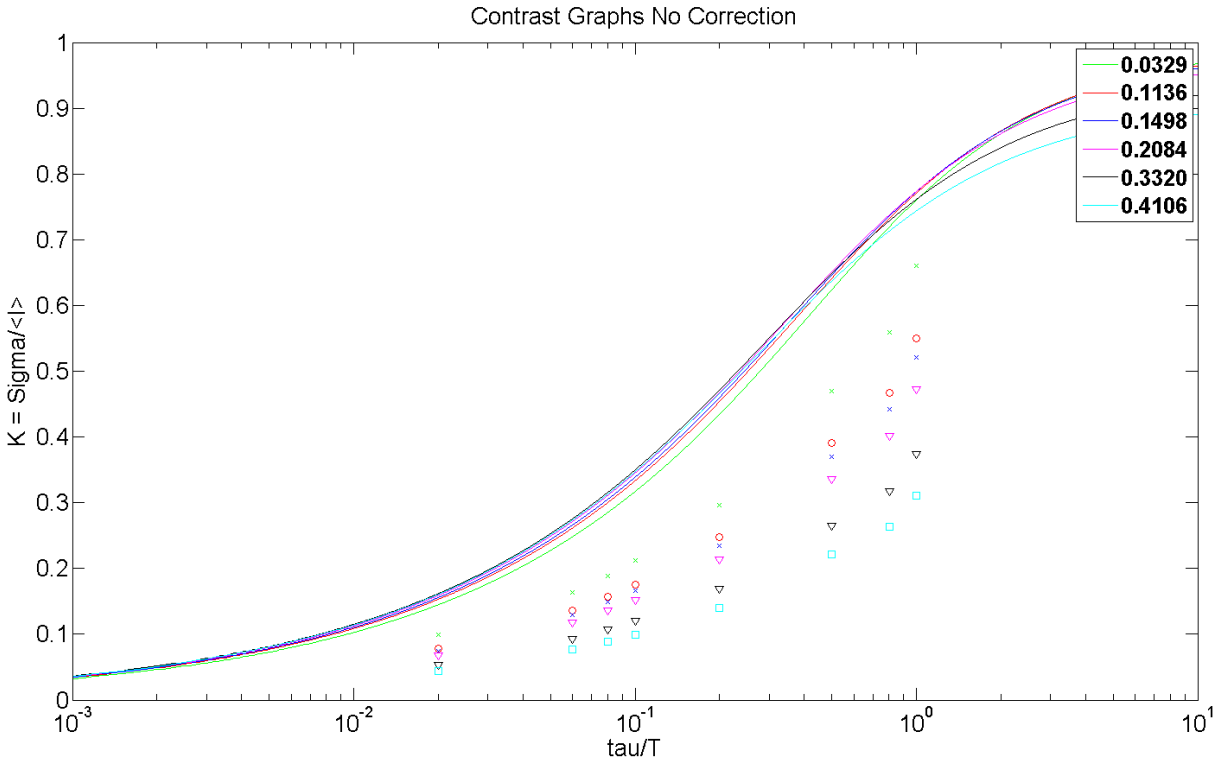

Figure 7 – Ratio of decorrelation time divided by exposure time graphed against dynamic contrast using the Lorentzian scattering model. Legend contains the estimated static contrast contribution. Plotted points are the simulated data and the plotted lines are the theoretical values.

Table 2: Percent error between simulated experiment and theory for standard Lorenztian distribution

	Percent Error (Exp – Theory)/Exp*100							
	τ_c/T							
ρ	**0.02**	**0.06**	**0.08**	**0.1**	**0.2**	**0.5**	**0.8**	**1**
0.0329	227.07	140.43	120.34	104.71	68.635	30.618	19.978	9.9104
0.117	374.6	209.85	178.62	157.44	103.55	50.087	33.175	22.122
0.1498	406.87	228.19	194.34	171.39	112.74	55.056	36.559	25.174
0.2084	457.42	256.79	218.81	193.02	127.15	62.882	41.904	30.031
0.332	542.14	304.66	260.02	229.49	151.54	76.493	51.323	38.756
0.4106	581.4	327.23	280.15	246.77	163.38	82.946	56.128	43.287

Not only did the error grow from the original DWS model as shown in Table 2, but the unexpected trend of a decreasing dynamic contrast with an increasing static contribution for the simulated data still existed (see Figure 7). Because of this, the behavior of the dLSI method was investigated under all possible cases of static contribution with a varying ρ.

3.2.3 Investigating the Dynamic Contrast Behavior

The formula relating the dynamic contrast to the mixed contrast and static contributions (Equation 7) was analyzed under a new range of ρ from 0 to 1. Figure 8 is a graphical representation of behavior of Equation 7 with a varying static contribution. Each graph in Figure 8 represents either a component of the dynamic contrast equation or the sum of its parts. Figure 8 (Top Left) is a representation of the intensity field autocorrelation function with a varying static contribution. Figure 8 (Top Right) is a representation of the electric field autocorrelation function as a function of varying static contribution. It should be noted that the (Top Left) and (Top Right) just described are the respective autocorrelation functions just mentioned multiplied by their ρ modifying terms (See Equation 7). Figure 8 (Bottom Left) is the sum of the intensity and field autocorrelation functions for a Lorentzian flow distribution. The (Bottom Right) is the same sum but with the DWS model applied.

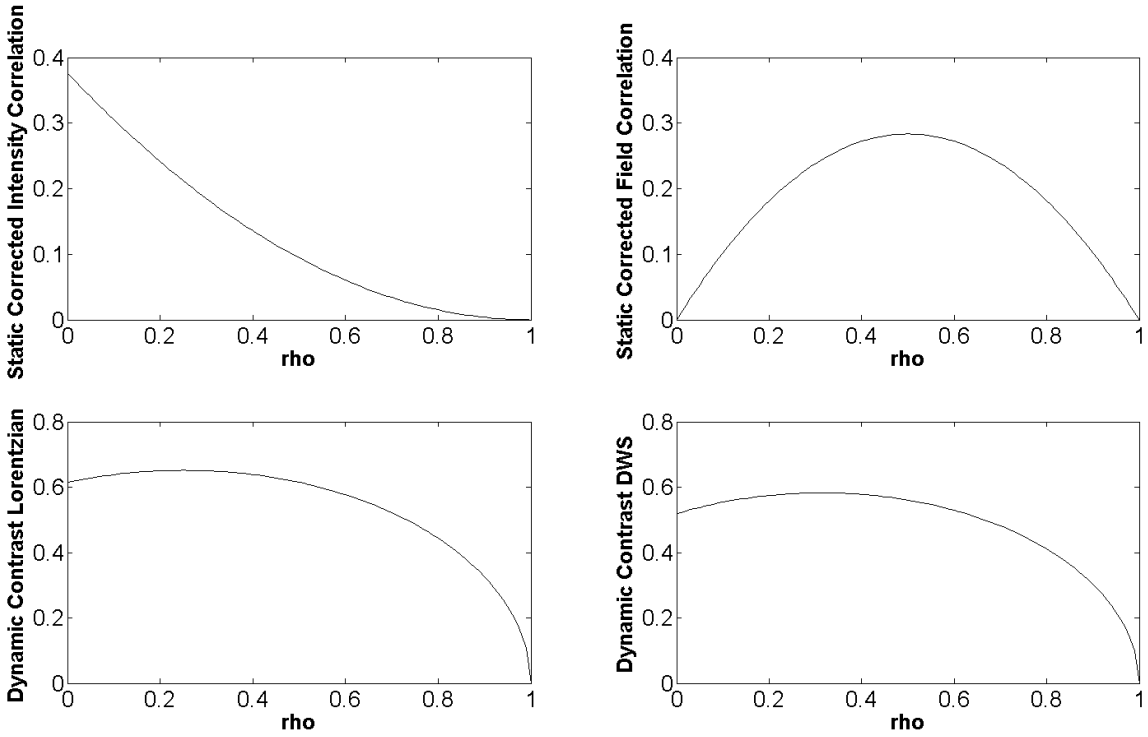

Figure 8 – Constituents of the dynamic contrast function. (Top Left) Intensity correlation function multiplied by $(1-\rho)^2$. (Top Right) Field correlation function multiplied by $2\rho(1-\rho)$. These are the constituents of Equation 7. (Bottom Left) Dynamic contrast as a function of ρ for τ_c/T = 0.5 considering a Lorenztian distribution. (Bottom Right) Dynamic contrast as a function of ρ for τ_c/T = 0.5 considering the DWS model.

The representation of Equation 7 as a function of ρ clearly demonstrates that, according to theory, the dynamic contrast increases in value initially then begins to decrease as the static contribution reaches approximately 0.4. These graphs were replicated for the extremes of this theory (τ_c/T between 0 and 1) and it was found that the behavior seen in Figure 8 is representative of the whole.

To compare this observation more closely to the observed behavior, the measured contrast and the dynamic contrast was compared as the static contribution was varied. Figure 9 shows the measured contrast is increasing with increasing static contribution while the dynamic contrast is always decreasing. Figure 9 displays this relationship for various ratios of τ_c/T.

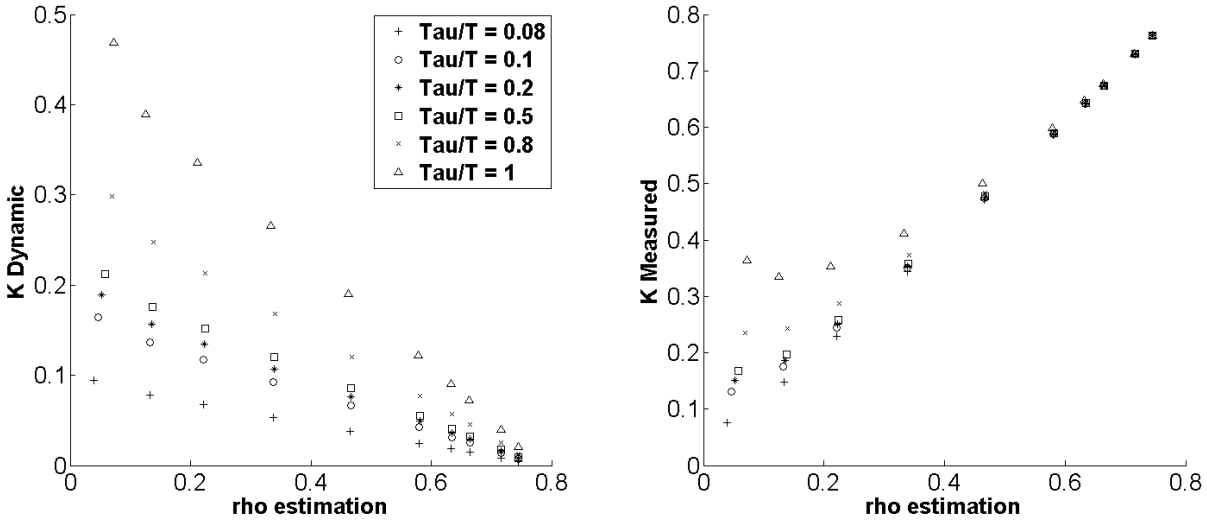

Figure 9 – Comparison of the measured and dynamic contrast from the dLSI algorithm. (Left) Dynamic contrast calculated by dLSI method. (Right) Measured contrast calculated by standard LASCA method. The legend lists the different ratios of τ_c/T for which the contrast as a function of ρ was estimated. It applies to both the measured and dynamic values.

As seen above in Figure 9, the measured contrast is increasing with an increasing static contribution. To simulate this, the value $\beta\rho^2$, where β is the maximal contrast obtainable by the system and ρ is the estimated static contribution, is added to Equation 7. This sum now represents the measured contrast that would be seen by a standard LASCA measurement. The observed departure from theory for the dynamic contrast could be due to the validity of the simulation algorithm. To verify that the simulation is behaving appropriately, the theory of summed independent speckle patterns needs to be addressed. This can be used to verify if the measured contrast is behaving appropriately and by association the simulation.

The sum of two independent speckle patterns produces a changing contrast profile if the ratio of the intensities is varied. [12] Figure 10 depicts the contrast of the two independent summed patterns just described.

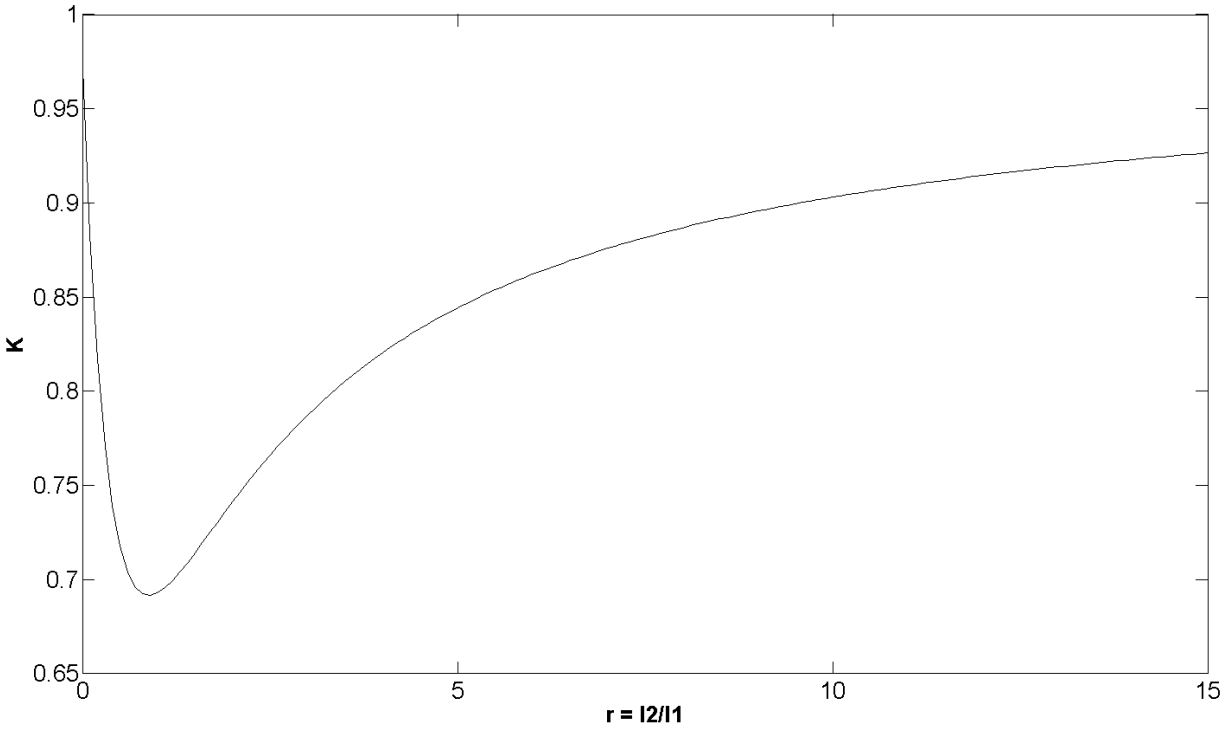

Figure 10 – Contrast behavior of the sum of two independent speckle patterns. The x-axis describes the ratios of the intensities of the speckle pattern. Equivalent intensities lead to a decrease in speckle contrast. When one pattern dominates the other the contrast begins to rise again. The y-axis is the observed contrast of the speckle sum.

If we let $r = \frac{I_2}{I_1}$, where r is the ratio of the speckle pattern intensities, then the contrast of the super-positioned speckle pattern behaves according to the plot in Figure 10. It can be seen that as r goes from 0 to approximately 2 the contrast decreases. [13] After this, I_2 begins to dominate the speckle pattern and the contrast begins to rise again and asymptotes to a contrast of 1. [13] This is seen in theory in Figure 10 and in simulation in the measured contrast plot in Figure 9. Although not entirely applicable due to one

pattern being dynamic, the theory should hold as the dynamic pattern becomes static for increasing values of τ_c/T. In Figure 9, when τ_c/T is equal to 1, this is readily apparent. The smaller the ratio of τ_c/T the more uniform the contrast; the addition of a secondary speckle pattern to this will start to only have an effect increasing effect on contrast. This is due to the dynamic pattern becoming a homogenous intensity without independent statistics to contribute to the speckle distribution. This phenomenon is also seen in Figure 9.

3.2.4 Formulation of an Empirically Fitted Algorithm

Now that the measured contrast behavior is justified, the dynamic contrast behavior needs to be reconciled, preferably while maintaining the dLSI algorithm procedures for the sake of consistency in calculation. The dynamic contrast is seen to be always decreasing with an increasing static contribution and is unvarying in this behavior. Rather than alter the algorithm to recalculate the static and dynamic contrasts, due to both time constrains and being outside the scope of this project, the consistent behavior of the dynamic contrast estimation was taken advantage of. To do this, two empirical modifying terms were introduced to influence the ρ terms that are modifying the intensity and field autocorrelation functions in Equation 7. Their effect is intended to force the dynamic contrast function into a solely inverse relationship with ρ.

The two modifying terms were obtained by performing and empirical fit using data from the simulations. Two scaling functions of the form $f\left(\frac{1}{\rho}\right) = \mathrm{B}(1)\left(\frac{1}{\rho}\right)^{\mathrm{B}(2)} + (\frac{1}{\rho})\mathrm{B}(3)$, where B(1,2,&3) are scalars, were introduced in a proper manner to avoid an ill conditioned system when fitting. The modifying terms are functions of $\frac{1}{\rho}$ for three

reasons: the relation between the decorrelation time and the dynamic contrast is heavily modified by ρ, it created a more stable system for fitting, and it helped reconcile the underestimation of the static contribution. To briefly touch upon the ρ underestimation, in Equations 5-7, ρ was defined as the ratio: $\frac{I_S}{I_D+I_S}$. During simulation for the data presented in Figure 9 the specified ρ's were: 0, 0.2, 0.33, 0.5, 0.67, 0.80, 0.86, 0.89, 0.94, and 0.97. The calculated ρ's were: 0.0637, 0.13, 0.22, 0.34, 0.47, 0.58, 0.63, 0.66, 0.72, and 0.74.

This method was able to modify the theory for the observed trend to produce single digit percent errors. Figure 11 shows the graph of the ratio of decorrelation time divided by exposure time against the dynamic contrast using the new empirical model. This graph can be referenced against Figure 7 to see the changes made. Table 3 lists the percent error between the new empirical relationship and simulation. Again, the rows correspond to different values of estimated static scattering and the columns refer to varying ratios of τ_c/T. One can see that the error is two orders of magnitude less than it previously was.

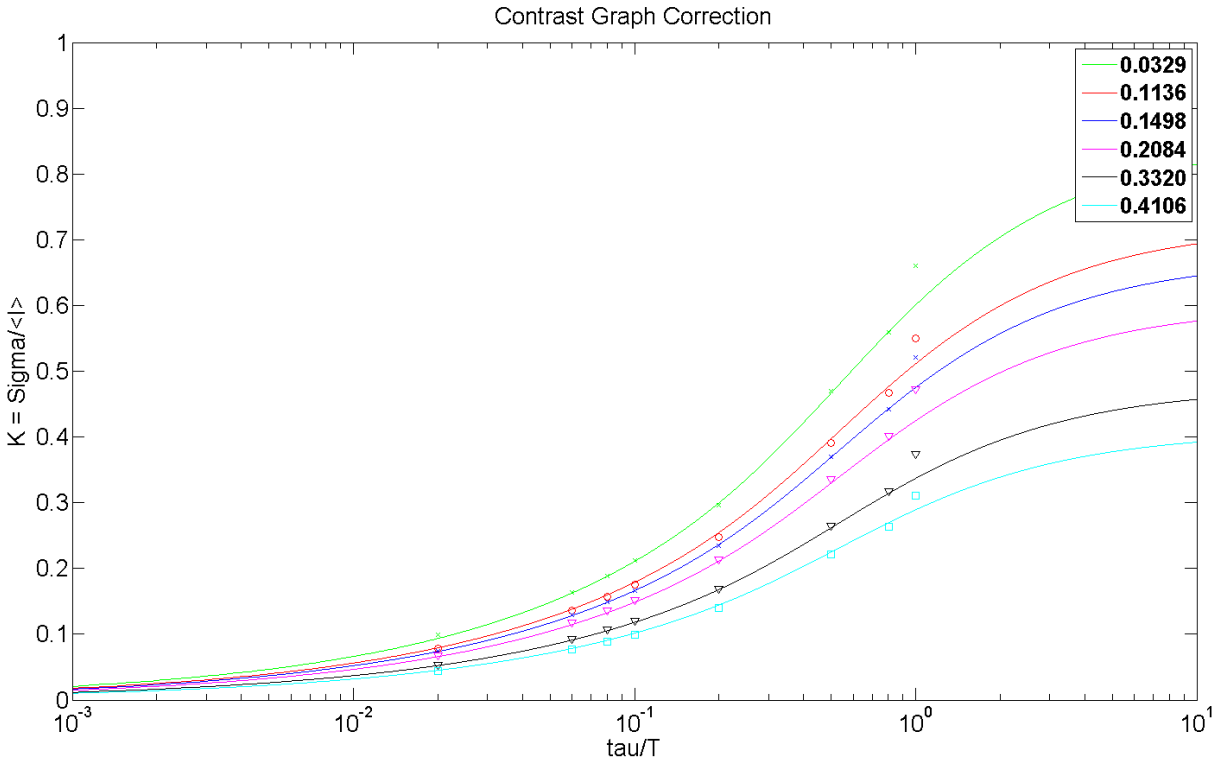

Figure 11 – Ratio of decorrelation time divided by exposure time graphed against dynamic contrast using the new empirically fit model. Legend contains the estimated static contrast contribution. Plotted points are the simulated data and the plotted lines are the theoretical values. Note the higher level of agreement between the theoretical lines and the simulation data for $\tau/T < 1$.

Table 3: Percent error between simulated experiment and theory for standard negative exponential autocorrelation model with power correction terms

	Percent Error (Exp – Theory)/Exp*100							
	τ_c/T							
ρ	**0.02**	**0.06**	**0.08**	**0.1**	**0.2**	**0.5**	**0.8**	**1**
0.0329	-29.34	-2.056	-0.6472	-1.3485	1.2874	-0.8151	0.0478	-6.035
0.117	2.3859	1.7551	1.3737	1.5648	2.7865	0.62043	0.7502	-4.217
0.1498	-3.057	-1.305	-1.2711	-0.7705	1.0073	-0.3721	-0.01038	-4.617
0.2084	-8.419	-4.432	-4.0403	-3.2773	-0.8434	-1.3801	-0.79592	-4.860
0.332	-4.968	-2.747	-2.5068	-2.0113	-0.2420	-0.7837	-0.42297	-3.662
0.4106	3.549	2.2574	2.5004	1.8251	2.3976	0.51764	0.7619	-2.154

3.3 Experimental Results

Both the DWS model of the autocorrelation function and the empirically adjusted model were used in the dLSI method to analyze the data gathered during experimentation. Figure 12 contains representative raw speckle images that were used in this analysis. They each contain a capillary tube with flowing milk on top of a static background tissue phantom. It can be seen that the areas of no flow have easily recognizable static speckle patterns while areas of flow are composed of homogenous intensities patterns.

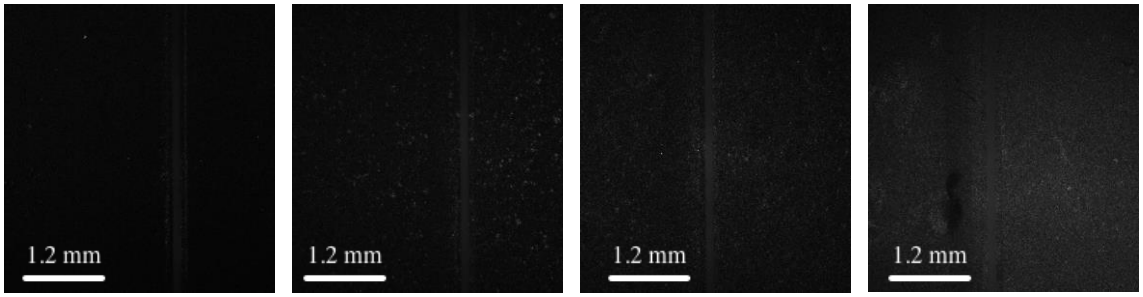

Figure 12 – Raw speckle images of milk with velocity 15 mm/s with varying background scattering. (Left) 0 mg/mL concentration of TiO_2 in PDMS (Middle Left) 0.5 mg/mL (Middle Right) 1 mg/mL (Right) 2 mg/mL

Some of the capillary tubes appear in different locations; this was accounted for by properly aligning the illuminating beam to be centered on the tube for each trial. Additionally, only the middle third of each image was used in analysis to help maximize the uniformity of the illuminating intensity.

3.3.1 Velocity to Decorrelation Time Relation

Figure 13 plots the programmed velocity on the x-axis and $1/\tau_c$ on the y-axis, with τ_c being the calculated decorrelation time that was extracted from the experimental images when using the DWS autocorrelation model. At low velocities (~1 – 15 mm/s) this should yield a linear relationship.

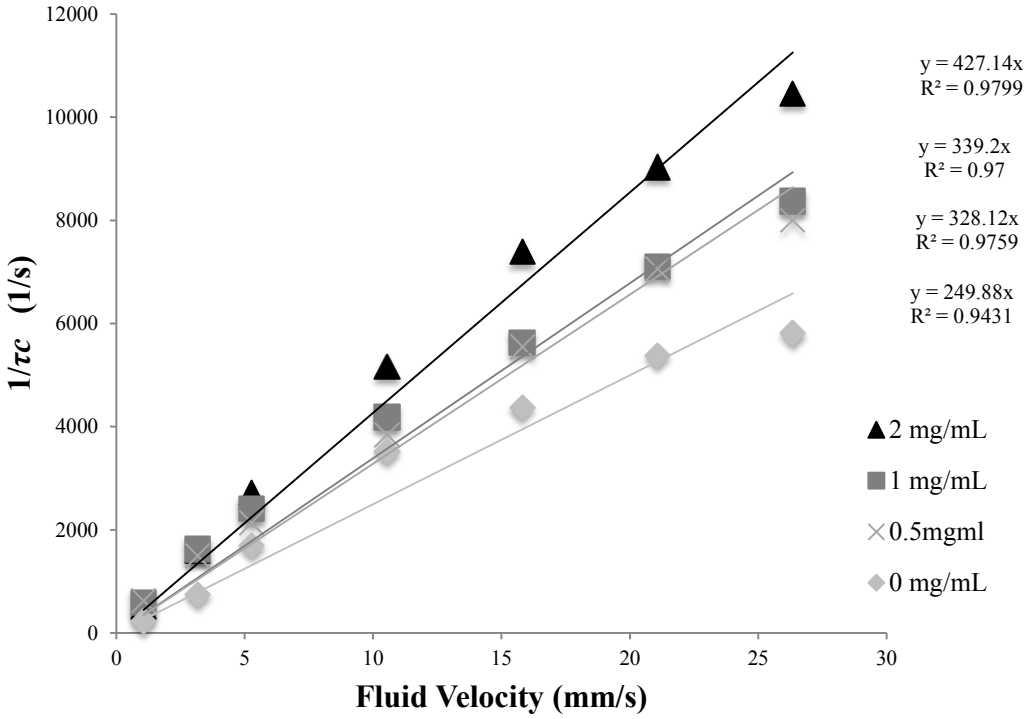

Figure 13 – Velocity to inverse correlation time comparison using the DWS scattering model. As expected lower velocities are related linearly and begin to become nonlinear at higher velocities.

The analysis was then repeated using the empirically adjusted model. The results obtained are shown in Figure 14. Both Figures 13 and 14 show the low velocity linear response assumption to be valid.

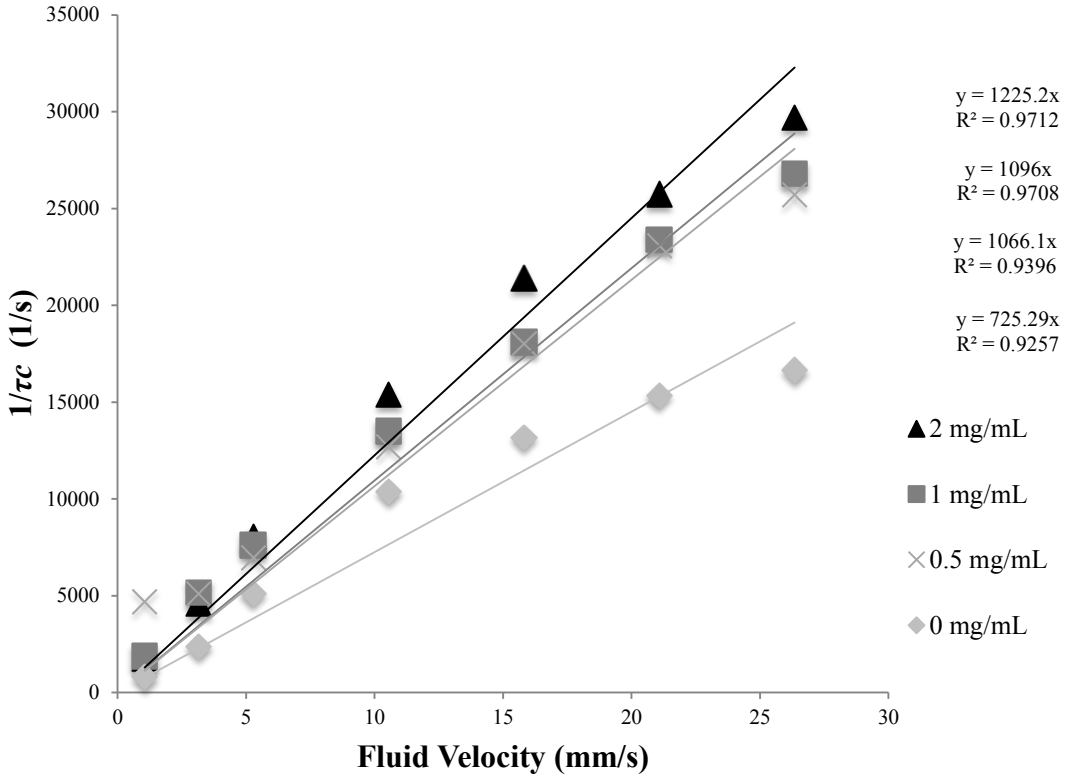

Figure 14 – Velocity to inverse correlation time comparison using the empirically fitted scattering model. As expected lower velocities are related linearly and begin to become nonlinear at higher velocities.

In both cases of experimental analysis, DWS and empirical, there were noticeable deviations between the slopes of the velocity-inverse tau curves when comparing backgrounds with different static scattering characteristics. Table 4 gives the percent differences between the 2 mg/ml scattering data points and the 1 mg/ml, 0.5 mg/ml, and 0 mg/ml for the DWS autocorrelation model analysis. Table 5 gives the same data for the empirical model analysis. Both Tables 4 and 5 shows that there was significant deviation between the 4 samples of scattering blocks. In both the DWS and the empirical fit the 0.5 mg/mL and the 1 mg/mL produces very similar values. However, when looking between the extremes of the 2 mg/mL and the 0 mg/mL blocks, there was on average ~50 %

difference. Perhaps the most notable feature is that both models share similar percent differences for the vast majority of comparisons.

Table 4: Percent difference between high scattering medium data points and its analogs for velocity ranges 1-25 mm/s using the DWS model

	Velocity (mm/s)						
Concentrations	**1**	**3**	**5**	**10**	**15**	**20**	**25**
2mg/ml-1mg/ml	-12.57	-2.27	11.29	18.94	23.85	21.39	19.934
2mg/ml-0.5mg/ml	-21.34	5.8857	21.20	25.56	24.90	21.80	23.43
2mg/ml-0mg/ml	55.14	52.74	37.39	31.92	40.85	40.45	44.37

Table 5: Percent difference between high scattering medium data points and its analogs for velocity ranges 1-25 mm/s using the empirical model

	Velocity (mm/s)						
Concentrations	**1**	**3**	**5**	**10**	**15**	**20**	**25**
2mg/ml-1mg/ml	-6.96	-12.87	5.60	12.33	15.44	9.15	9.76
2mg/ml-0.5mg/ml	-169.02	-11.36	13.65	17.52	15.91	10.32	13.47
2mg/ml-0mg/ml	53.65	47.83	36.57	32.51	38.40	40.44	43.87

3.3.2 Probability Density Function Analysis of Background Scattering Phantoms

The speckle patterns caused by the background of each scattering block were analyzed based on their probability density functions (PDFs) as functions of normalized intensity. This was done to ensure that the scattering properties of the blocks did not exhibit any obscure behavior, i.e a normal distribution or a uniform distribution with even intensity across all values. It can be seen in Figure 15 that the blocks are exhibiting Rayleigh distributed intensity patterns, which is the result of multiple scatterings of photons in the material. The effects of the Rayleigh distribution are noted by its influence

of the contrast value's maximum asymptote, effectively lowering the maximum attainable contrast. [13]

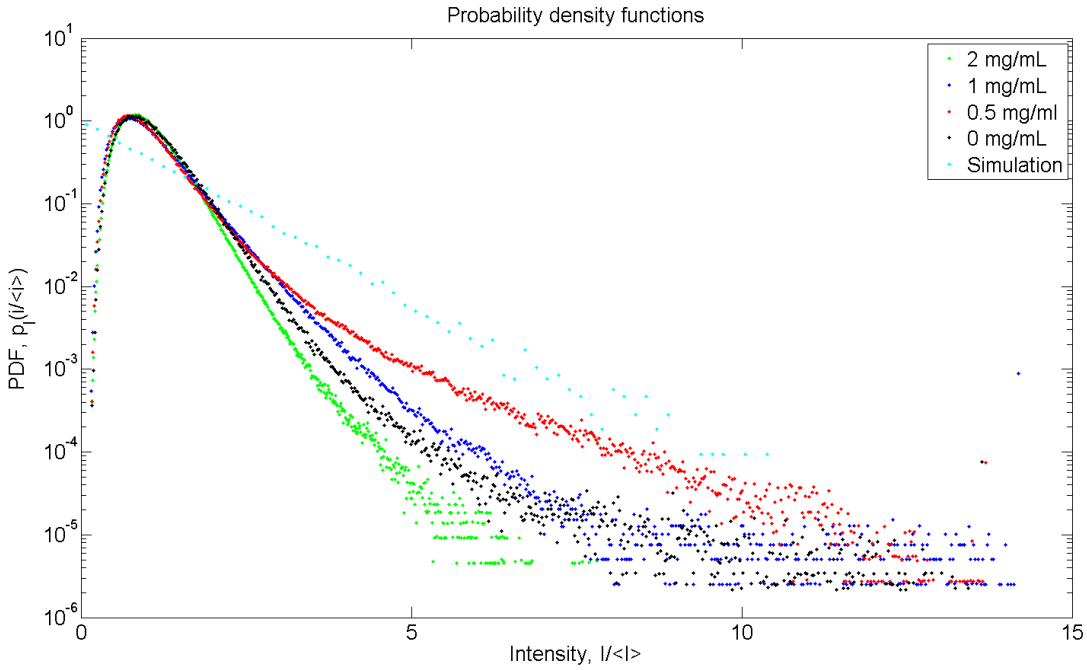

Figure 15– Intensity PDFs representative of the behavior of the various scattering blocks used in this experiment. The legend lists the concentrations of scattering agent in the PDMS blocks causing the speckle PDF and the simulation with a negative exponential intensity distribution.

When the PDFs are normalized by their mean intensities, as shown in Figure 15, they display similar distributions. Variations do exist in the distribution, altering the contrast, which is expected due to the varying concentrations of scattering agent dissolved in the PDMS blocks. The simulation serves to compare what an intensity PDF would look like in a single scattering case. Recognizing that the distributions were similarly shaped led to an assurance that each block had appropriate scattering characteristics. The simulated data distribution in Figure 15, which is represented by the

cyan points, is a negative exponential distribution. This means it is considering a single scattering case and is expected to differ from the multiply scattering blocks.

Chapter 4: Discussion

4.1 Discussion Overview

The results exhibited behavior that was atypical of the hypothesis presupposed by the dLSI method. Both the DWS and the empirical model were not able to accurately resolve decorrelation times over different backgrounds, and showed increasing error as the background's average intensity dropped. The following discussion will outline what the possible causes for this disagreement are and possible avenues of investigation for correction.

4.2 Simulation and Experimentation

Simulation provided the insight necessary to evaluate what was observed in the experimental model. It led to a greater understanding of the relationship between the dLSI method's calculations of decorrelation times with a varying static contribution. The DWS model for calculating decorrelation times and the empirical model employed both produced very similar results when used to analyze experimental data. The slopes of the velocity to inverse decorrelation times, although numerically different, shared similar percent differences between the 2 mg/mL scattering background and all other backgrounds when analyzed within their respective methods. It can be seen that at higher velocities the empirical model provided noticeably lower percent differences when compared to the DWS model, but this is irrelevant when the larger issues are considered. A possible explanation for the similar percent differences is that the static contribution to the contrast did not vary to a large degree. Further analysis of the data shows this to be true, with a minimum of 0.039 and a maximum of 0.054. The variation in the curve

relating contrast to decorrelation time produced by the range of static contributions observed is miniscule between those two values. An explanation for this behavior will follow in section 4.5.

4.3 Multiple Scattering Events

The case of the multiple scatterings affecting the estimation of the contrast, and thus the correlation times, is proven and cannot be ignored. The empirical model relies on a negative exponential distribution of scattering intensities. This formulation is satisfactory when imaging media that exhibit single scattering phenomena, however, biological media often produce multiple scatterings. [13] It is necessary to recognize that the contrast is no longer bounded between 0 and 1 for a completely Rayleigh distributed pattern but between 0 and $1/\sqrt{2}$. [13] The new bound is due to a Rayleigh distribution, which is the superposition of two independent equal intensity speckle patterns. The upper bound is effectively made lower because the speckle pattern begins to overlap and create a more homogenous intensity pattern. [11] There does not seem to be any accounting for the emergence of a static Rayleigh distribution in the static contrast estimation of dLSI, only single scattering static contribution. It is possible this lowers or somehow alters the estimated static contribution, something that was observed, which would have effects on the dynamic estimation.

The temporal response, which arises from the time series averaging of contrast images, is also altered by the occurrence of Rayleigh distributed scatterers and requires more frames to achieve maximum contrast. [13] This effect on the temporal contrast is shown in Figure 16.

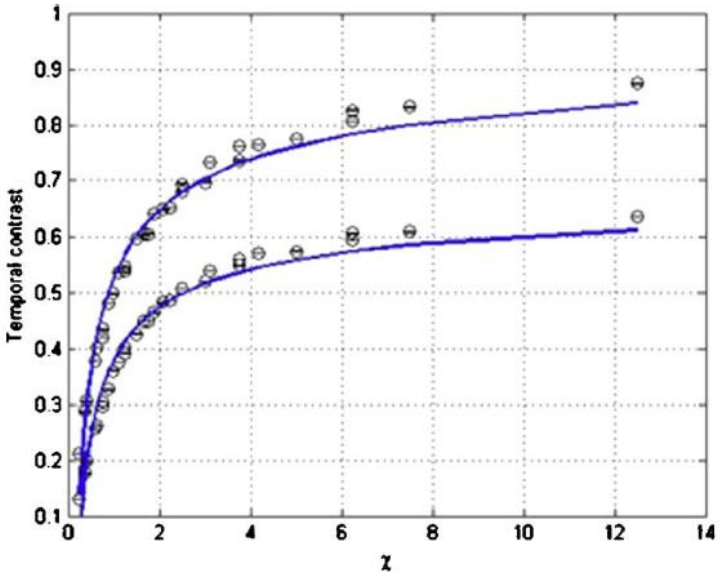

Figure 16 – Temporal contrast accounting for Rayleigh scattering. The top curve is using a negative exponential intensity distribution and the bottom is using a Rayleigh intensity distribution. The x-axis is in arbitrary time shift units and the y-axis is the temporal contrast. [13]

Notice in Figure 16 that the temporal contrast for a Rayleigh pattern, the bottom curve, asymptotes to a smaller value and takes longer achieve its asymptote. The x-axis in Figure 16 represents the number of frames averaged together, while the y-axis represents the contrast produced by this averaging. It is important to consider this because the dLSI method makes use of a similar temporal averaging scheme.

A simple solution can be offered to the multiple scattering dilemmas. It can be shown that the PDFs of speckle functions are Fourier transformations of their autocorrelation functions. [9] Convolving their PDFs gives a joint PDF that represents both patterns. The resulting autocorrelation function of the joint PDF is a simple product of the independent autocorrelation functions. [9] This can be used to model a mixture of Brownian and ordered flow processes as well as correct for multiple scattering events. [9] It should be remembered that the DWS formulation accounts for multiple scattering

events; however, in the form used, it only considers the case of Brownian motion and is not fully suitable for the analysis done in this experiment.

4.4 Physical Relationship between Decorrelation and Velocity

To relate back to an earlier discussion about the physical relationship between decorrelation time and particle velocity, up until recently largely speculative models were being imposed. Equation 9 demonstrates one such relationship. A phase screen model has been proposed that demonstrates the speckle correlation autocoefficient can be modeled as a simple airy function. [8] A brief formulation of this model is described in Equation 10.

$$\frac{C_i(\tau)}{\mu_i^2} = \left(\frac{2J_1\left(\frac{\pi DV\tau}{\lambda d_o}\right)}{\frac{\pi DV\tau}{\lambda d_o}}\right)^2 = \left(\frac{2J_1\left(\frac{\tau}{\tau_r}\right)}{\pi\frac{\tau}{\tau_r}}\right)^2 \tag{10}$$

$$\tau_r = \frac{PSF}{V} \qquad PSF \sim \frac{\lambda d_o}{D}$$

V describes the velocity of the object plane and D is the pupil diameter, in a subjective case the imaging aperture, d_o is the distance from the pupil to the image plane, μ_i^2 is the square of the average intensity, τ_r is the characteristic decorrelation time, τ is the correlation time variable, and λ is the wavelength of the coherent light. Using a ratio of $\frac{d_o}{D}$ ~ 10, which is an f-stop of 10 and characteristic of the imaging system used, and a wavelength equal to 640 nm we find that the *PSF* ~ 6.64e-6 m. After accounting for

magnification of the lens, the slope relating $1/\tau_r$ to V is ~15000. This is a value that is not observed in this experiment. Deviation is expected because Equation 10 is formulated for single dynamic surface scattering speckle patterns, not the multiple scattering patterns being investigated.

4.5 Causes of Inconsistency

After investigating the possible causes for the inconsistencies, the choices have been narrowed to a few. It is believed that the cause for the similar percent differences between the DWS and the empirical model is due to little variation in the estimation of the static contrast contribution. This is likely attributed to the high scattering properties of the dynamic medium, cow's whole milk. Another factor is that while other researchers implanted their dynamic media into a statically scattering environment, the dynamic media was superficial in this experiment and obscured static scattering from behind.

To lend credibility to this claim, when the simulation was run with no static component dLSI estimated a static contrast of 0.0329. This confirmed that the experimental trial is also predicting little to no static component. Figure 9 shows that the intensity distributions are of the same form but have different variances, meaning that their static contribution is unlikely to be the same and small. The last variable in the system is the overall intensity of the background speckle and the intensity of the dynamic media. As the mean intensity of the background scattering elevated, the mean intensity of the dynamic scattering component rose as well. This all occurs with little to no change in the static contrast contribution.

Two things contributed to lack of change in the static component estimation: milk is a host of variable size particles that exhibit greater Brownian motion than this method was intended for, and the possible effects of refractive glass between the static scattering and dynamic media. By using laser diffraction, milk is reported to have a distribution of colloidal particles on the order of a $1/10^{th}$ to $1/6^{th}$ the size of red blood cells. [16] This would raise the diffusion coefficient of the dynamic media meaning the constituent particles would undergo random motion at a greater speed. This would have the effect of randomizing, to a larger degree, the scattering directions of photons from the background over time due to changing spatial relations between the scattering colloidal particles. The capillary tube may also have been acting as a cylindrical lens refracting scattered light in close proximity to the capillary tube into the milk. Explaining the rise in scattering intensity without a rise in static scattering contribution to the contrast is now possible. The higher than anticipated levels of Brownian motion could have caused background-scattered light to become decorrelated from the background and essentially dynamic. The extra static scattering not only appeared dynamic but caused the dynamic pattern to become brighter (as observed) due to the additional light. Recalling from Equation 2, contrast is inversely proportional to intensity and directly proportional to the variance of the speckle intensity. The apparent increase in intensity in conjunction with an either stationary or lowered variance, assuming both patterns are dynamic on relatively equal orders, created the observed lowering of the contrast.

Chapter 5: Conclusion

The dynamic method has been investigated in its simplest form through both simulation and experimentation. Completely Lorentzian flow was not able to be resolved in simulation so the implementation of an empirical equation was made. After reducing error to a minimum, both the DWS and empirical model were applied to the experimental data. The results showed that little to no change in the static contribution was accompanied by a decrease in dynamic contrast as concentration of the scattering agent was increased. Under the conditions of 1 mg/ml and 0.5 mg/ml the measured decorrelation times agreed with little error, but the decorrelation times could not be resolved over the span from 0 to 2 mg/ml. A theory was offered as an explanation regarding this but requires further investigation to validate it. This paper will hopefully extend to other researchers the application of this method under various extremes of conditions.

5.1 Future Work

This work provided a basis for investigating the extent to which dLSI can resolve dynamic speckle contrast when obscured by static speckle patterns. Although useful insights have been made here, there are still many aspects of this project that can be further investigated. Characterization of the dLSI method over a wider range of background scattering components would be necessary to provide more expansive experimental results. Designing background scattering surfaces that range between 0 and 1 for their static scattering contrasts would be ideal, allowing for a full range analysis. Creating a sub-surface dynamic scattering medium as well as performing the experiment

with a dynamic medium that has more similar scattering characteristics to the background would also be of great importance. As discussed earlier, the milk was so highly scattering it obscured the speckle pattern from the background. Bringing the scattering properties of the dynamic and static medium into closer alignment would help eliminate this. The sub-surface dynamic scattering would also help alleviate the masking of the static pattern by ensuring that the static scattering agent is always directly visible. It should be remembered that the masking of the static scattering was an issue in this experiment because the backgrounds were still contributing intensity to the dynamic medium, but they appeared to be themselves dynamic due to the high scattering of the milk.

The speckle simulation could also be investigated in greater detail. It is still possible the simulation was improper even though it satisfied the independent speckle sum criteria. This is a concern because the dLSI theory should be predicting dynamic contrast in accordance with Figure 8, which for small static contributions does not greatly vary. It instead predicted what appeared to be the relative percentage of dynamic contrast to static contrast in the image. It is possible that in the process of simulating the mixed speckle images some higher order statistical properties of the image were degraded. A more sophisticated algorithm for generating joint speckle patterns with varying decorrelation times could be used if this is the case. One method that exists for this is known as the copula, which takes advantage of joint speckle distribution theory proposed in the discussion, and may be of particular interest in furthering this project. [8]

To summarize the steps necessary to continue: the design of experimental background scatters must be expanded, the dynamic media must be made to have scattering properties more closely aligned with the background, the dynamic scatters

should be deep to the static scattering components, and the speckle simulation algorithm must be revisited in greater detail and perhaps use a more complex simulation technique. These steps outline what is necessary to further research into quantitative laser speckle imaging using the dLSI static scattering estimation algorithms. This method has shown promise in the ability to create repeatable trends in simulated data, continuing this work should prove its effectiveness in experimentation over a greater range of conditions.

Bibliography

1. Boas, D. a, & Dunn, A. K. (2010). Laser speckle contrast imaging in biomedical optics. Journal of Biomedical Optics, 15(1), 011109. doi:10.1117/1.3285504

2. Briers, J. D. (2001). Laser Doppler, speckle and related techniques for blood perfusion mapping and imaging. Physiological Measurement, 22(4), R35–66. Retrieved from http://www.ncbi.nlm.nih.gov/pubmed/11761081

3. Briers, J. D., & Webster, S. (1996). Laser speckle contrast analysis (LASCA): a nonscanning, full-field technique for monitoring capillary blood flow. Journal of Biomedical Optics, 1(2), 174–179.

4. Cheng, H., Luo, Q., Liu, Q., Lu, Q., Gong, H., & Zeng, S. (2004). Laser speckle imaging of blood flow in microcirculation. Physics in Medicine and Biology, 49(7), 1347–1357. doi:10.1088/0031-9155/49/7/020

5. Choi, B., & Kim, J. (2012). Methods to Enhance Laser Speckle Imaging of High-Flow and Low-Flow Vasculature. Conf Proc IEE Eng Med Biol Soc, 4073–4076. doi:10.1109/IEMBS.2009.5333204.Methods

6. Choi, B., Ramirez-San-Juan, J. C., Lotfi, J., & Stuart Nelson, J. (2006). Linear response range characterization and in vivo application of laser speckle imaging of blood flow dynamics. Journal of Biomedical Optics, 11(4), 041129. doi:10.1117/1.2341196

7. Draijer, M., Hondebrink, E., van Leeuwen, T., & Steenbergen, W. (2009). Review of laser speckle contrast techniques for visualizing tissue perfusion. Lasers in Medical Science, 24(4), 639–651. doi:10.1007/s10103-008-0626-3

8. Duncan, D. D., & Kirkpatrick, S. J. (2008a). Algorithms for simulation of speckle (laser and otherwise), 6855, 685505–685505–8. doi:10.1117/12.760518

9. Duncan, D.D., Kirkpatrick, S.J. (2010). Can laser speckle flowmetry be made a quantitative tool? NIH Public Access, 32(15), 2188–2190.

10. Dunn, A. K., Bolay, H., Moskowitz, M. A., & Boas, D. A. (2001). Dynamic Imaging of Cerebral Blood Flow Using Laser Speckle, 195–201.

11. Fercher, A. F., & Briers, J. D. (1981). Flow visualization by means of single-exposure speckle photography. Optics Communications, 37(5), 326–330.

12. Forrester, K. R., Tulip, J., Leonard, C., Stewart, C., & Bray, R. C. (2004). A Laser Speckle Imaging Technique for Measuring Tissue Perfusion, 51(11), 2074–2084.

13. Goodman, JW. Speckle Phenomena In Optics. Roberts & Company; 2008

14. Kirkpatrick, S. J., Duncan, D. D., Wang, R. K., & Hinds, M. T. (2007). Quantitative temporal speckle contrast imaging for tissue mechanics. Journal of the Optical Society of America. A, Optics, Image Science, and Vision, 24(12), 3728–34. Retrieved from http://www.ncbi.nlm.nih.gov/pubmed/18059925

15. Meisner, J. K., Sumer, S., Murrell, K. P., Higgins, T. J., & Price, R. J. (2012). Laser speckle flowmetry method for measuring spatial and temporal hemodynamic alterations throughout large microvascular networks. Microcirculation (New York, N.Y. : 1994), 19(7), 619–31. doi:10.1111/j.1549-8719.2012.00197.x

16. Milk Fat Size Distribution by Laser Diffraction. (n.d.). Retrieved May 06, 2014, from https://www.beckmancoulter.com/wsrportal/bibliography?docname=BCPCS002_LE.pdf

17. Nadkarni, S. K., Bouma, B. E., Helg, T., Chan, R., Halpern, E., Chau, A., Tearney, G. J. (2005). Characterization of atherosclerotic plaques by laser speckle imaging. Circulation, 112(6), 885–92. doi:10.1161/CIRCULATIONAHA.104.520098

18. Nadort, A., Woolthuis, R. G., van Leeuwen, T. G., & Faber, D. J. (2013). Quantitative laser speckle flowmetry of the in vivo microcirculation using sidestream dark field microscopy. Biomedical Optics Express, 4(11), 2347–61. doi:10.1364/BOE.4.002347

19. Parthasarathy, A. B., Tom, W. J., Gopal, A., Zhang, X., & Dunn, A. K. (2008). Robust flow measurement with multi-exposure speckle imaging. Optics Express, 16(3), 1975–1989.

20. Richards, L. M., Kazmi, S. M. S., Davis, J. L., Olin, K. E., & Dunn, A. K. (2013). Low-cost laser speckle contrast imaging of blood flow using a webcam. Biomedical Optics Express, 4(10), 2269–83. doi:10.1364/BOE.4.002269

21. Saleh, B. E. A., Teich, M. C., & Wiley, C. J. (1991). Statistical optics 10.1 (Vol. 5, pp. 342–383).

22. Thompson, O., Andrews, M., & Hirst, E. (2011). Correction for spatial averaging in laser speckle contrast analysis. Biomedical Optics Express, 2(4), 1021–1029.

23. Völker, a, Zakharov, P., Weber, B., Buck, F., & Scheffold, F. (2005). Laser speckle imaging with an active noise reduction scheme. Optics Express, 13(24), 9782–7. Retrieved from http://www.ncbi.nlm.nih.gov/pubmed/19503186

24. Xu, C. F. C. and M. L. and N. Y. Z. and S. Y. T. and H. S. S. and Z. Z. (2004). Speckle intensity correlation in the diffraction region near rough surfaces and simulational experiments for extraction of surface parameters. EPL (Europhysics Letters), 65(6), 779. Retrieved from http://stacks.iop.org/0295-5075/65/i=6/a=779

25. Yuan, S., Devor, A., Boas, D. A., & Dunn, A. K. (2005). Determination of optimal exposure time for contrast imaging, 44(10), 1823–1830.

26. Zakharov, P., & Andreas, V. (2013). Quantitative modeling of laser speckle imaging.Optical Society of America, 8–11.

27. Zakharov, P., Völker, a C., Wyss, M. T., Haiss, F., Calcinaghi, N., Zunzunegui, C., … Weber, B. (2009). Dynamic laser speckle imaging of cerebral blood flow. Optics Express, 17(16), 13904–17. Retrieved from http://www.ncbi.nlm.nih.gov/pubmed/19654798

Appendix A: dLSI Algorithm Demonstration

The following excerpt describes how the dLSI method is implemented. It first calculates the standard measured contrast, it then estimates the static contribution from a series of images, and then using the static contrast knowledge estimates the dynamic contrast. [27]

1. Calculate the measure contrast: $K_m = [\frac{<I^2>}{<I>^2} - 1]^{1/2}$, where <…> denotes the spatial averaging over a selected area containing N pixels: $< I > = \frac{1}{N}\sum_{i=1}^{N} I(x_i)$ and $< I^2 > = \frac{1}{N}\sum_{i=1}^{N} I^2(x_i)$. We have denoted this measured contrast with an index *m* ($K_m = K$)

2. Estimate the static contribution from the two sequential images $I_1(x_i)$ and $I_2(x_i)$ with $i = 1 \ldots N$ defining the same set of pixels as used in step 1: $\rho = \frac{1}{\beta^{1/2}}[\frac{<I_1 I_2>}{<I_1><I_2>} - 1]^{1/2}$, where $< I_1 >< I_2 > = \frac{1}{N}\sum_{i=1}^{N} I_1(x_i) I_2(x_i)$. The β-factor used in this calculation has to be obtained separately. It can be calibrated using a solid white medium such as a block of Teflon or a sheet of paper with $\rho = 1$.

3. With knowledge of ρ the mixed dynamic contrast K can be obtained with the following relationship $K^2 = K_m^2 - \beta\rho^2$. Using the appropriate relation for the correlation function of the electric field, the correlation time can be extracted."

Appendix B: Simulated Speckle Images

The following section contains all images needed to be representative of the set of speckle images generated and used for calculation in this experiment. Each figure contains a set of images for the given ratios of τ_c/T: 0.02, 0.06, 0.08, 0.1, 0.2, 0.5, 0.8, and 1. The static contribution in each figure varies from 0 to 32 times the intensity of the dynamic contribution. Each figure also contains a pure static speckle image for reference.

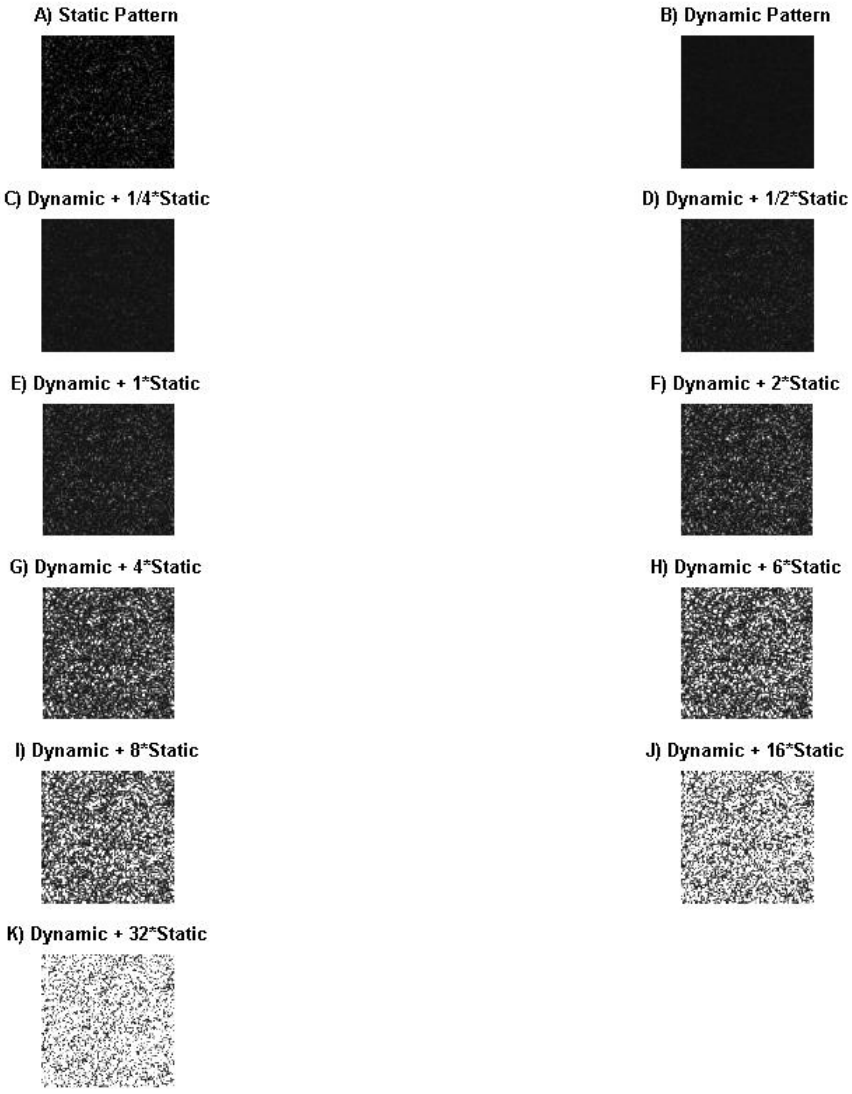

Figure 17 – Simulated speckle patterns with varying static contribution for the decorrelation time to exposure time ratio τ_c/T = 0.02. A) Static pattern no dynamic speckle B) Dynamic pattern no static speckle C) Dynamic + ¼*Static Pattern D) Dynamic + ½*Static Pattern E) Dynamic + 1*Static Pattern F) Dynamic + 2*Static Pattern G) Dynamic + 4*Static Pattern H) Dynamic + 6*Static Pattern I) Dynamic + 8*Static Pattern J) Dynamic + 16*Static Pattern K) Dynamic + 32*Static Pattern

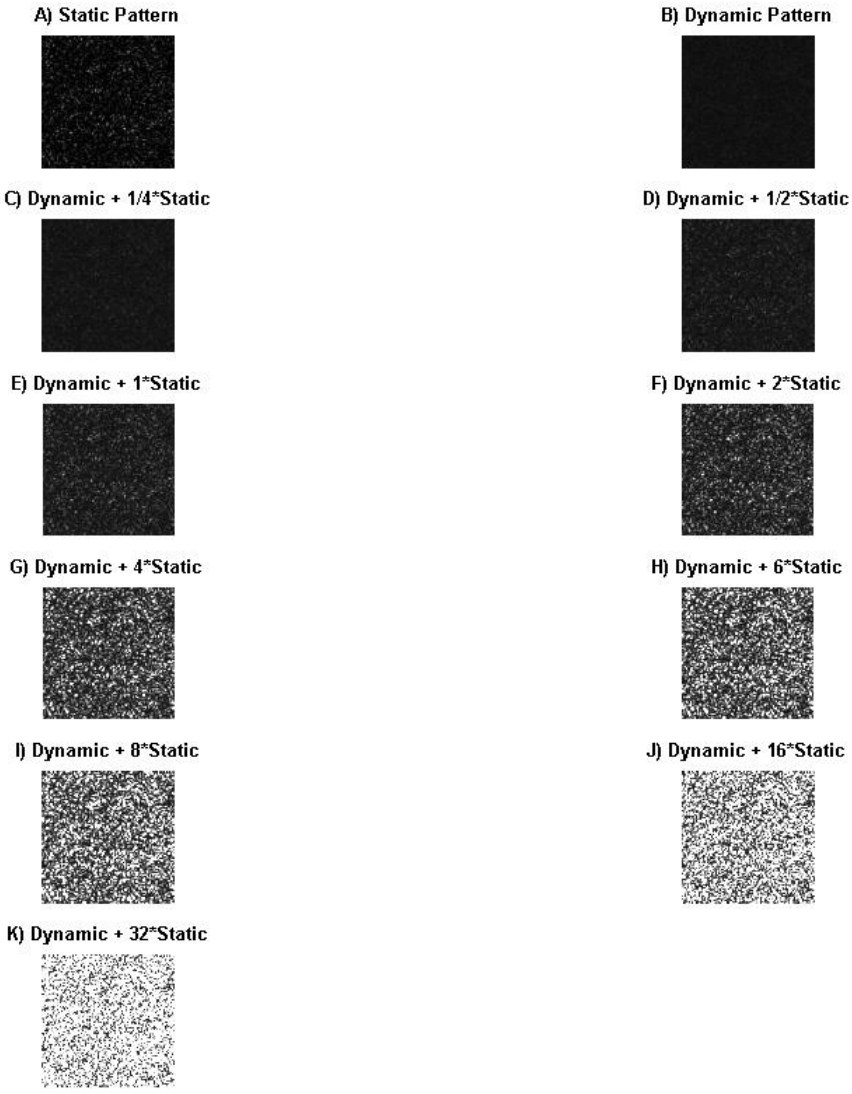

Figure 18 – Simulated speckle patterns with varying static contribution for the decorrelation time to exposure time ratio τ_c/T = 0.06. A) Static pattern no dynamic speckle B) Dynamic pattern no static speckle C) Dynamic + ¼*Static Pattern D) Dynamic + ½*Static Pattern E) Dynamic + 1*Static Pattern F) Dynamic + 2*Static Pattern G) Dynamic + 4*Static Pattern H) Dynamic + 6*Static Pattern I) Dynamic + 8*Static Pattern J) Dynamic + 16*Static Pattern K) Dynamic + 32*Static Pattern

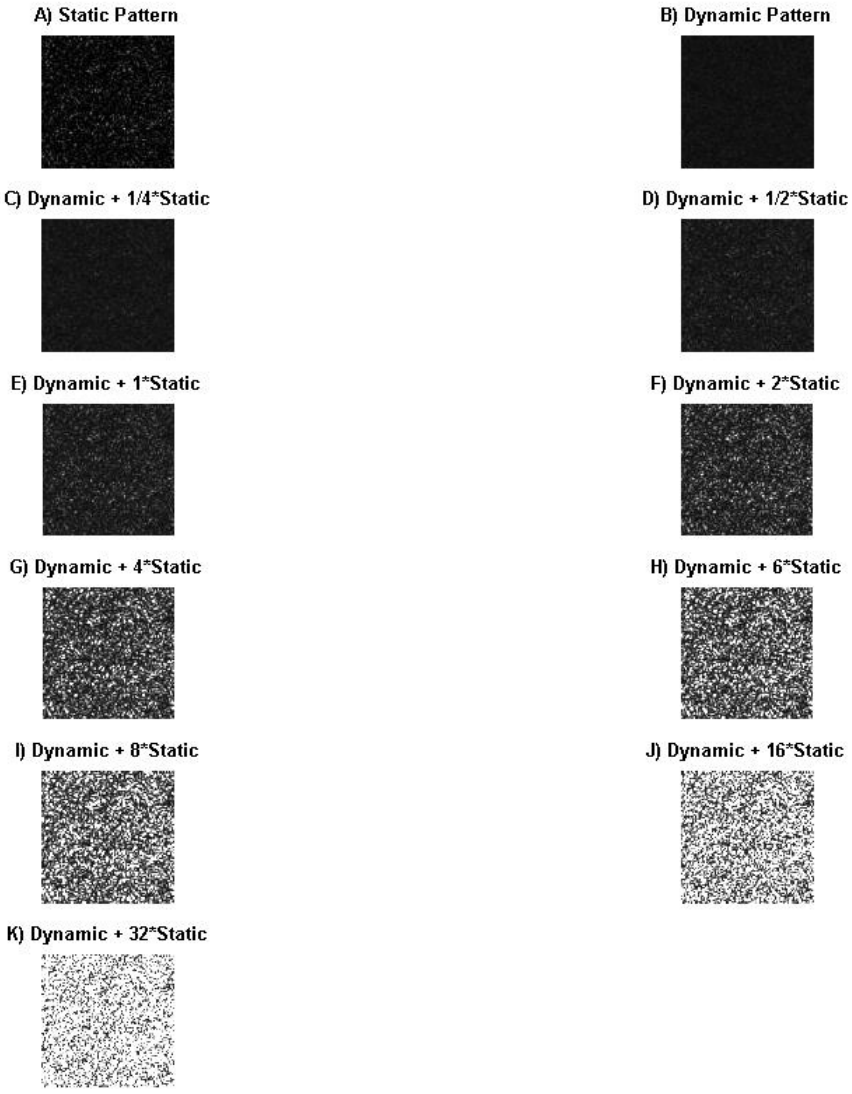

Figure 19 – Simulated speckle patterns with varying static contribution for the decorrelation time to exposure time ratio τ_c/T = 0.08. A) Static pattern no dynamic speckle B) Dynamic pattern no static speckle C) Dynamic + ¼*Static Pattern D) Dynamic + ½*Static Pattern E) Dynamic + 1*Static Pattern F) Dynamic + 2*Static Pattern G) Dynamic + 4*Static Pattern H) Dynamic + 6*Static Pattern I) Dynamic + 8*Static Pattern J) Dynamic + 16*Static Pattern K) Dynamic + 32*Static Pattern

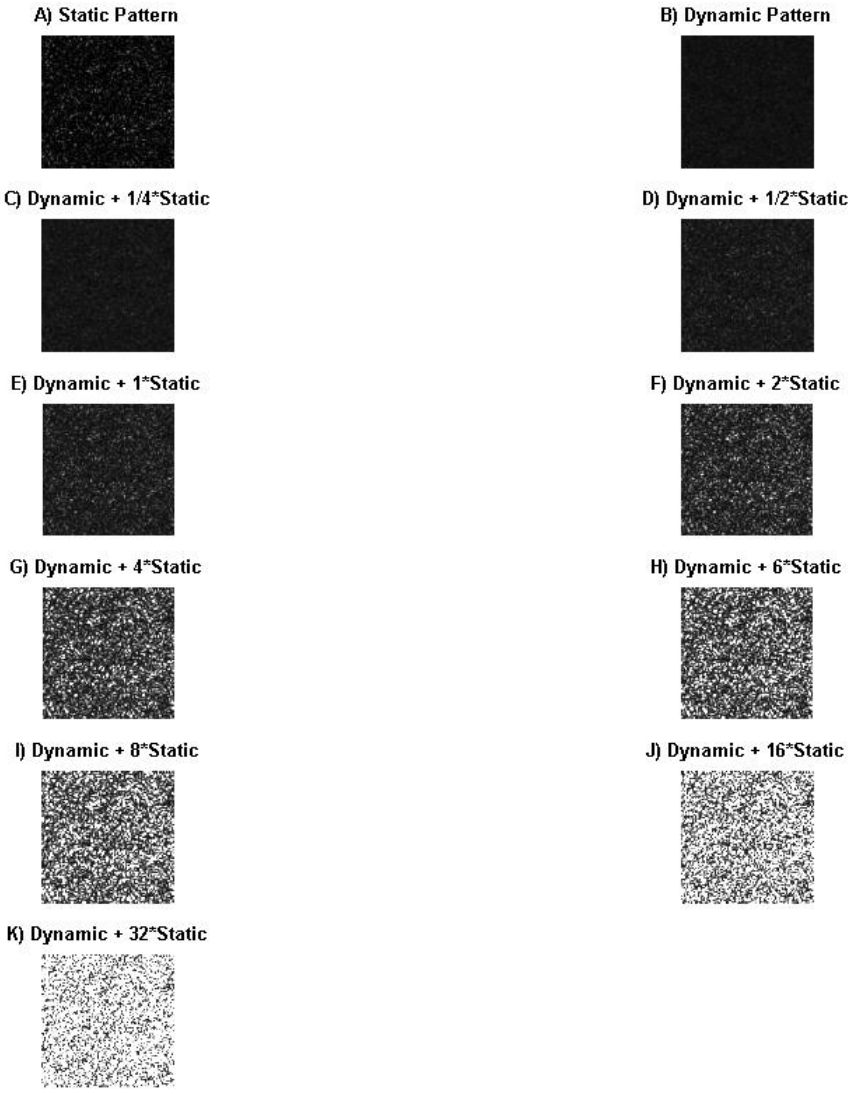

Figure 20 – Simulated speckle patterns with varying static contribution for the decorrelation time to exposure time ratio $\tau_c/T = 0.1$. A) Static pattern no dynamic speckle B) Dynamic pattern no static speckle C) Dynamic + ¼*Static Pattern D) Dynamic + ½*Static Pattern E) Dynamic + 1*Static Pattern F) Dynamic + 2*Static Pattern G) Dynamic + 4*Static Pattern H) Dynamic + 6*Static Pattern I) Dynamic + 8*Static Pattern J) Dynamic + 16*Static Pattern K) Dynamic + 32*Static Pattern

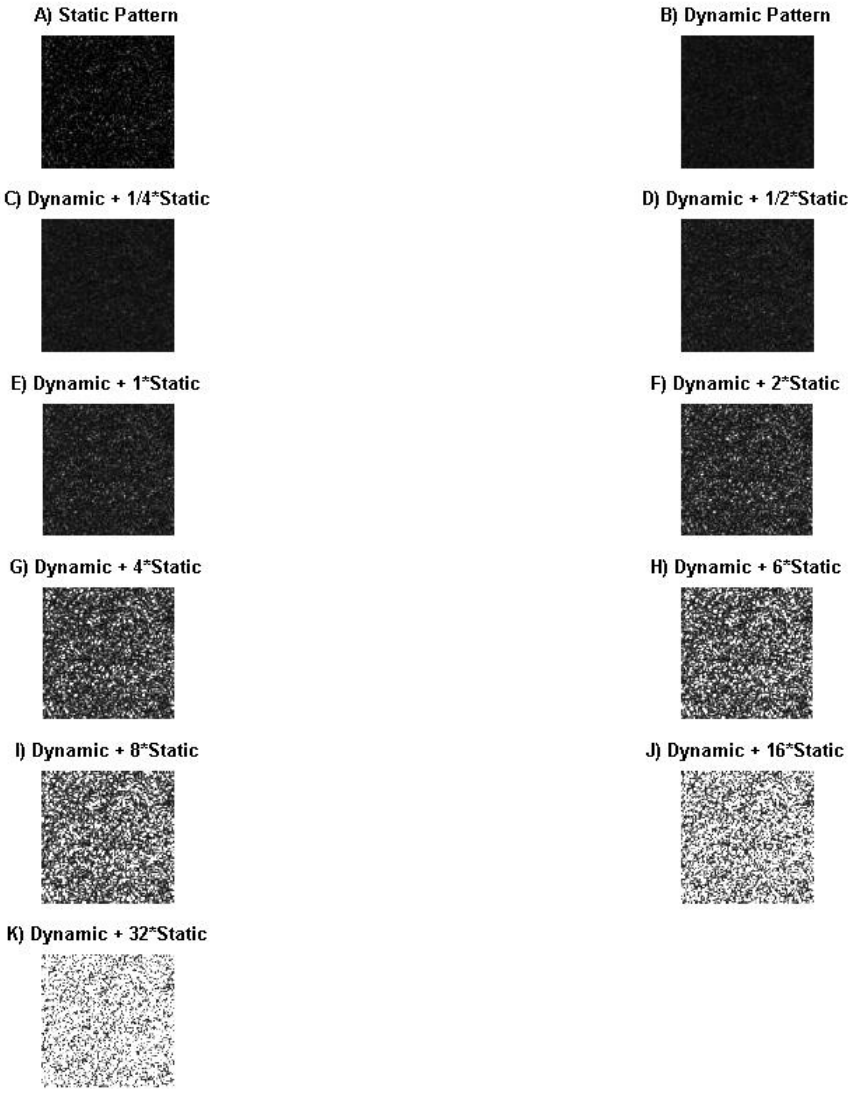

Figure 21 – Simulated speckle patterns with varying static contribution for the decorrelation time to exposure time ratio $\tau_c/T = 0.2$. A) Static pattern no dynamic speckle B) Dynamic pattern no static speckle C) Dynamic + ¼*Static Pattern D) Dynamic + ½*Static Pattern E) Dynamic + 1*Static Pattern F) Dynamic + 2*Static Pattern G) Dynamic + 4*Static Pattern H) Dynamic + 6*Static Pattern I) Dynamic + 8*Static Pattern J) Dynamic + 16*Static Pattern K) Dynamic + 32*Static Pattern

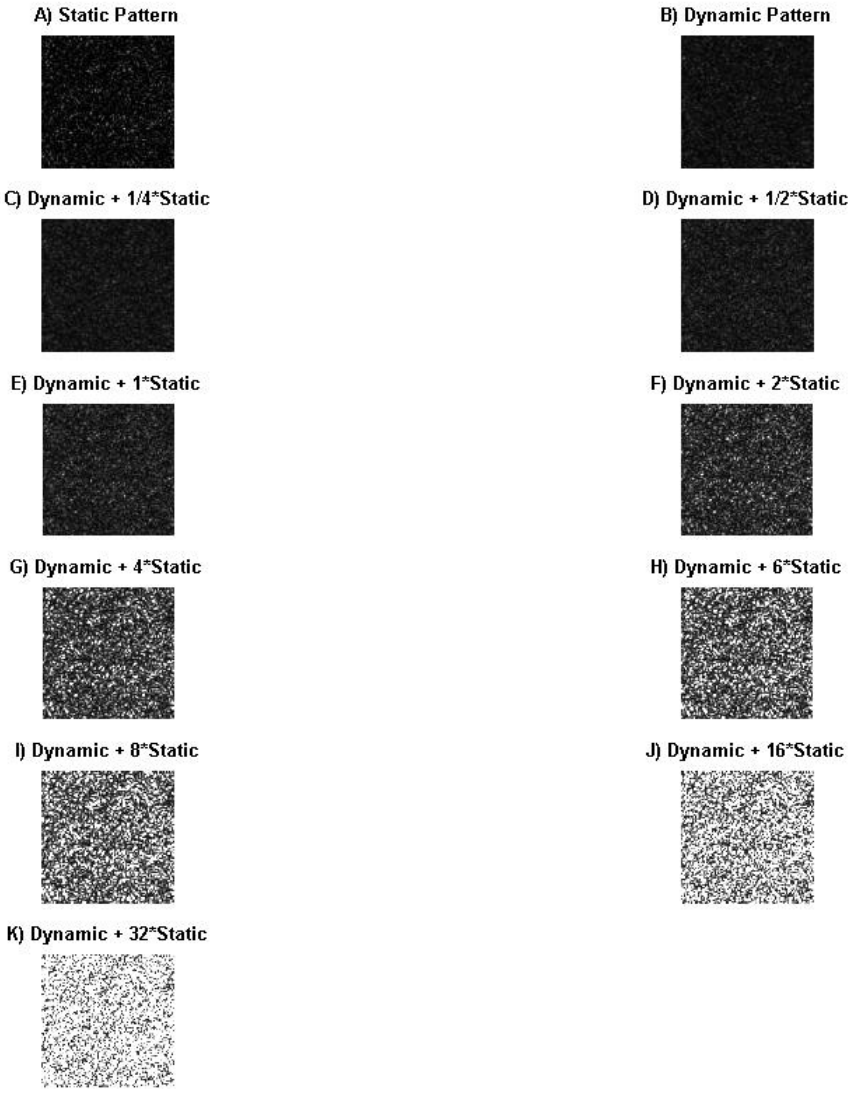

Figure 22 – Simulated speckle patterns with varying static contribution for the decorrelation time to exposure time ratio $\tau_c/T = 0.5$. A) Static pattern no dynamic speckle B) Dynamic pattern no static speckle C) Dynamic + ¼*Static Pattern D) Dynamic + ½*Static Pattern E) Dynamic + 1*Static Pattern F) Dynamic + 2*Static Pattern G) Dynamic + 4*Static Pattern H) Dynamic + 6*Static Pattern I) Dynamic + 8*Static Pattern J) Dynamic + 16*Static Pattern K) Dynamic + 32*Static Pattern

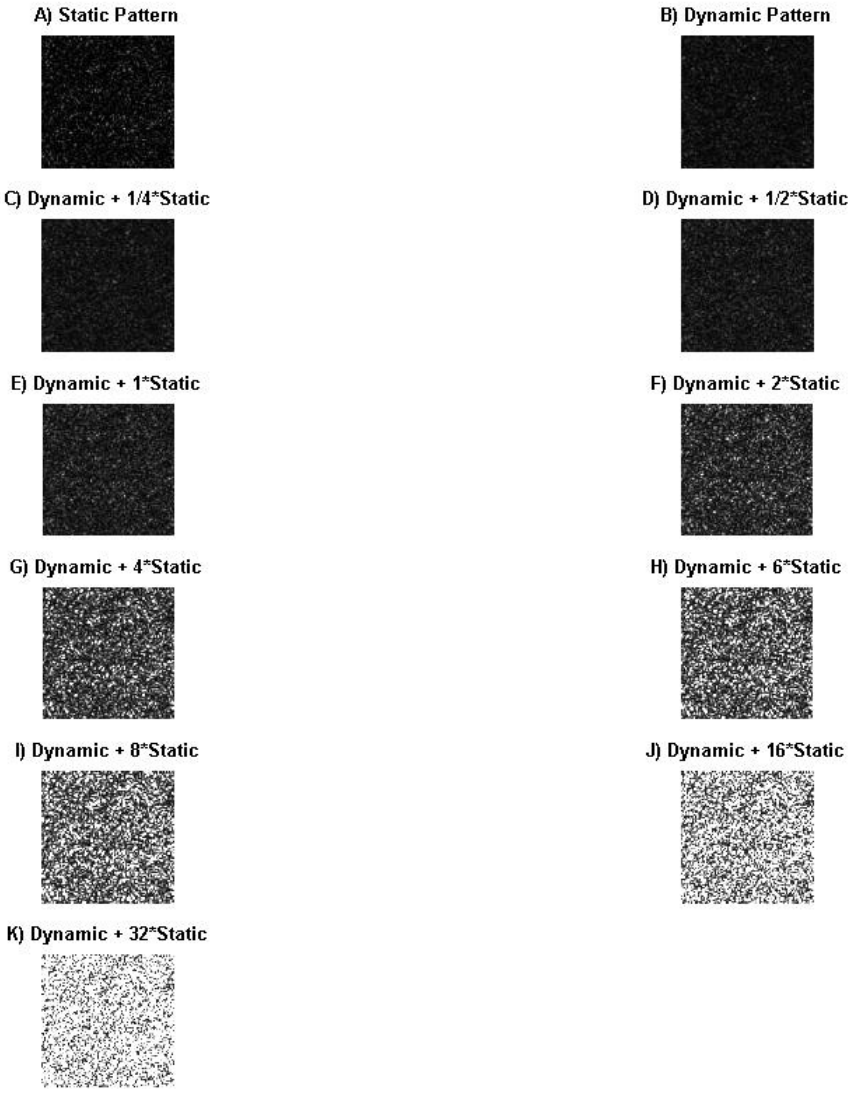

Figure 23 – Simulated speckle patterns with varying static contribution for the decorrelation time to exposure time ratio $\tau_c/T = 0.8$. A) Static pattern no dynamic speckle B) Dynamic pattern no static speckle C) Dynamic + ¼*Static Pattern D) Dynamic + ½*Static Pattern E) Dynamic + 1*Static Pattern F) Dynamic + 2*Static Pattern G) Dynamic + 4*Static Pattern H) Dynamic + 6*Static Pattern I) Dynamic + 8*Static Pattern J) Dynamic + 16*Static Pattern K) Dynamic + 32*Static Pattern

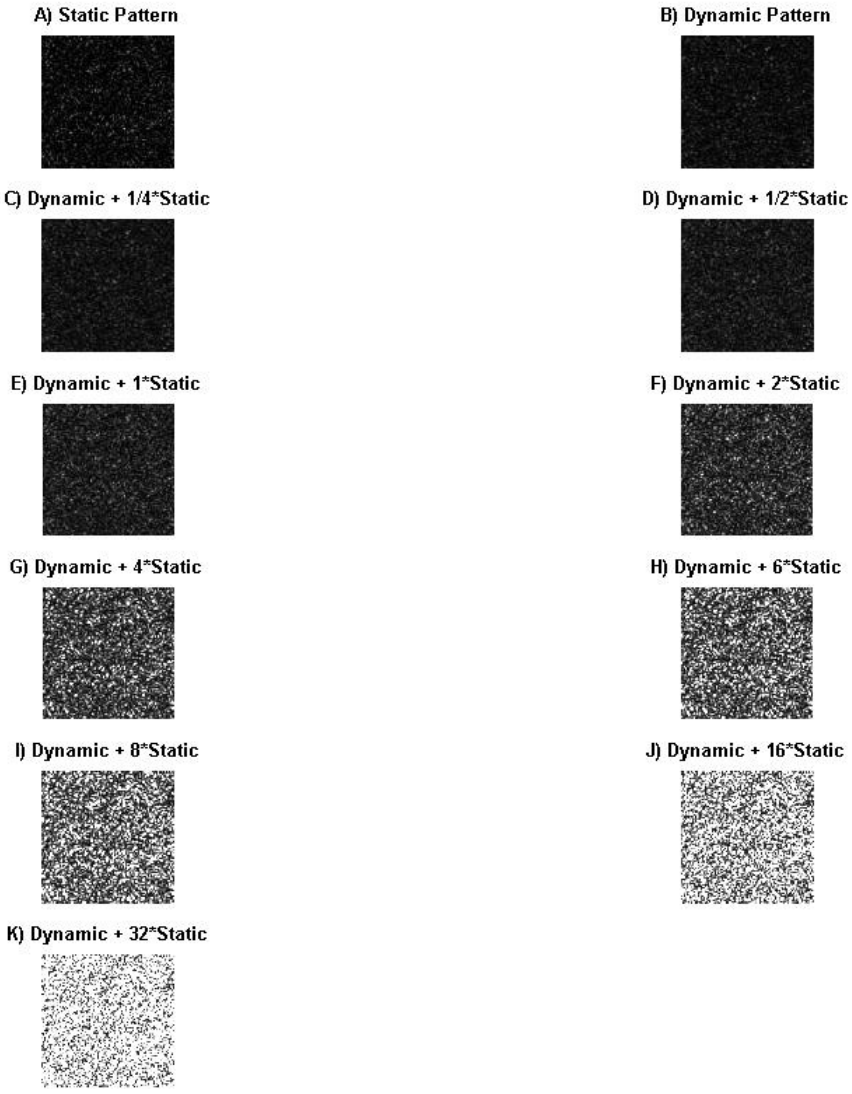

Figure 24 – Simulated speckle patterns with varying static contribution for the decorrelation time to exposure time ratio $\tau_c/T = 1$. A) Static pattern no dynamic speckle B) Dynamic pattern no static speckle C) Dynamic + ¼*Static Pattern D) Dynamic + ½*Static Pattern E) Dynamic + 1*Static Pattern F) Dynamic + 2*Static Pattern G) Dynamic + 4*Static Pattern H) Dynamic + 6*Static Pattern I) Dynamic + 8*Static Pattern J) Dynamic + 16*Static Pattern K) Dynamic + 32*Static Pattern

Appendix C: Raw Speckle Images

The following section contains sets of raw speckle images that are representative of the images acquired and used for analysis in this experiment for the scattering blocks of 0 mg/ mL, 0.5 mg/mL, 1 mg/mL, and 2 mg/mL for flow rates of 1 mm/s, 3 mm/s, 5 mm/s, 10 mm/s, 15 mm/s, 20 mm/s, and 25 mm/s. The area in each image is approximately 64 mm^2 under a 10X magnification.

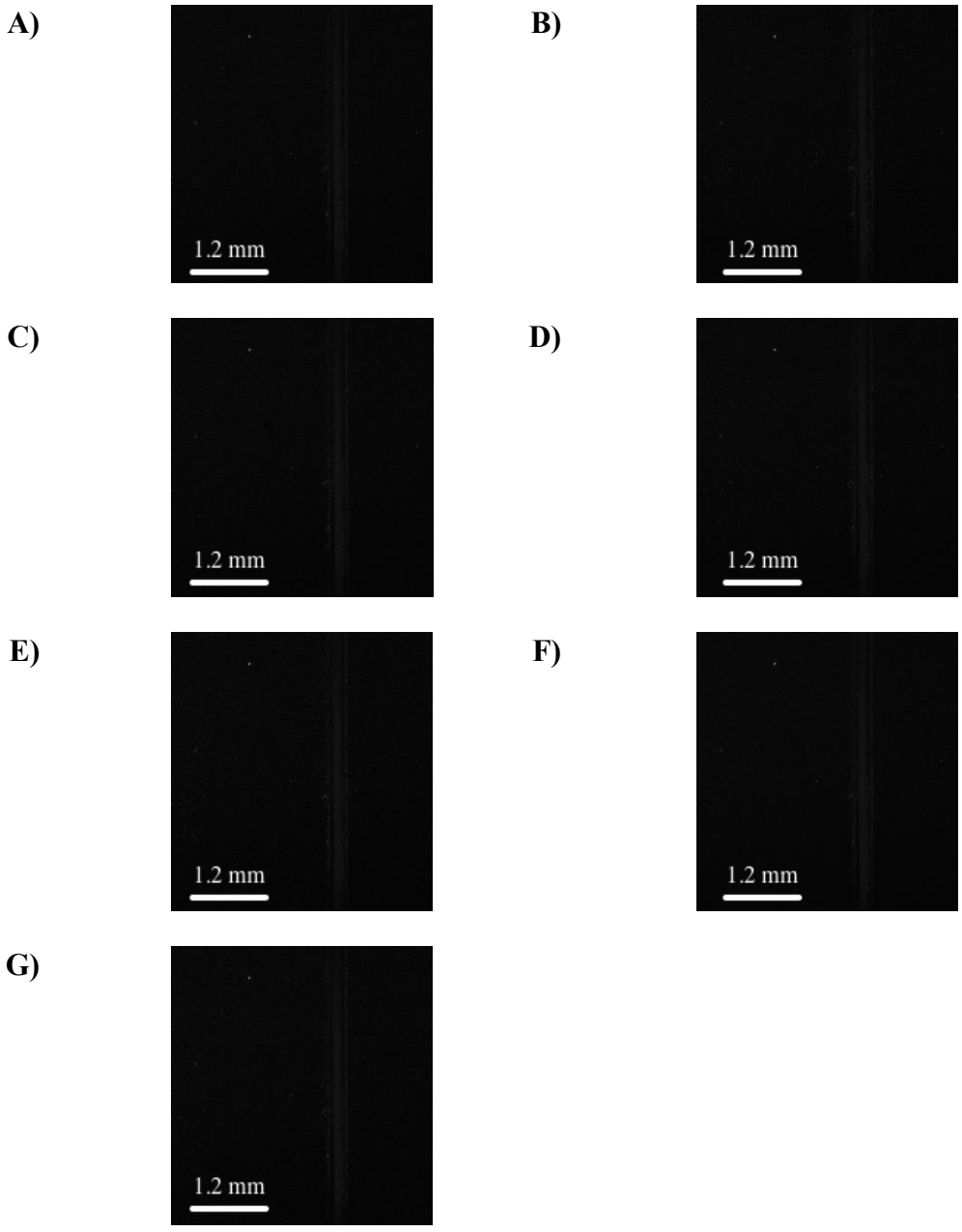

Figure 25 – Raw speckle images acquired by CCD camera for 0 mg/mL TiO_2 to PDMS background scattering. A) 1 mm/s flow B) 3 mm/s flow C) 5 mm/s flow D) 10 mm/s flow E) 15 mm/s flow F) 20mm/s flow G) 25 mm/s flow

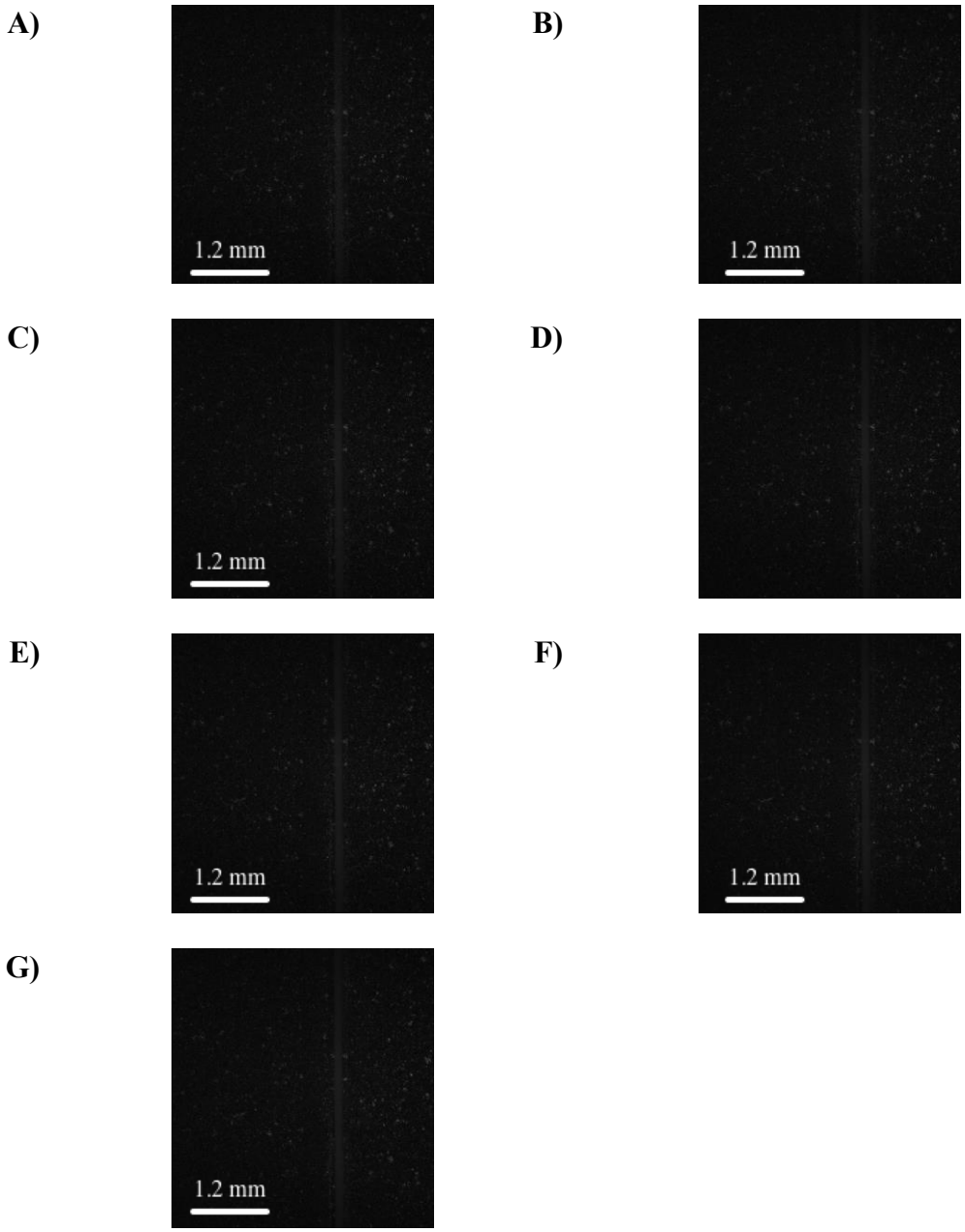

Figure 26 – Raw speckle images acquired by CCD camera for 0.5 mg/mL TiO_2 to PDMS background scattering. A) 1 mm/s flow B) 3 mm/s flow C) 5 mm/s flow D) 10 mm/s flow E) 15 mm/s flow F) 20mm/s flow G) 25 mm/s flow

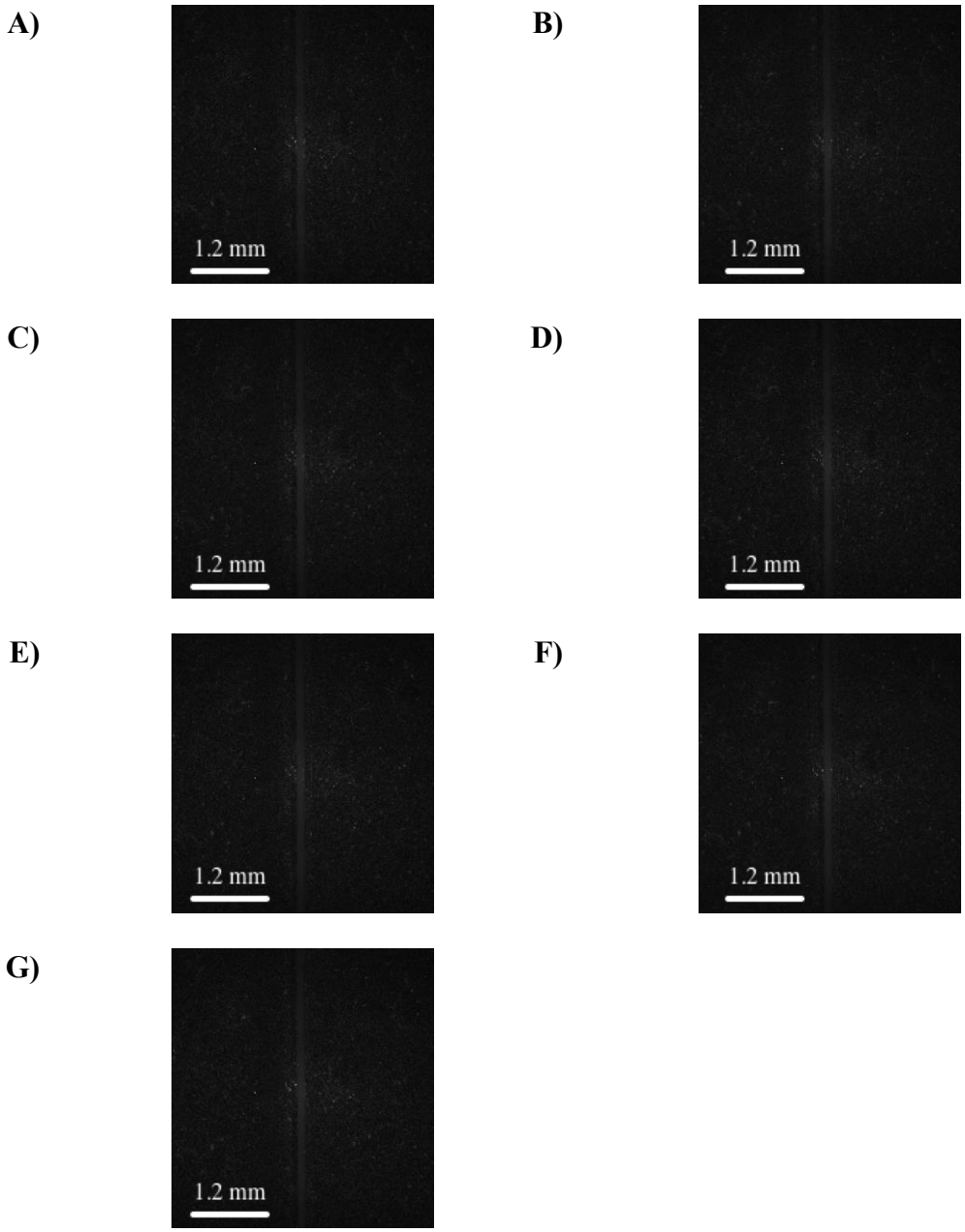

Figure 27 – Raw speckle images acquired by CCD camera for 1.0 mg/mL TiO_2 to PDMS background scattering. A) 1 mm/s flow B) 3 mm/s flow C) 5 mm/s flow D) 10 mm/s flow E) 15 mm/s flow F) 20mm/s flow G) 25 mm/s flow

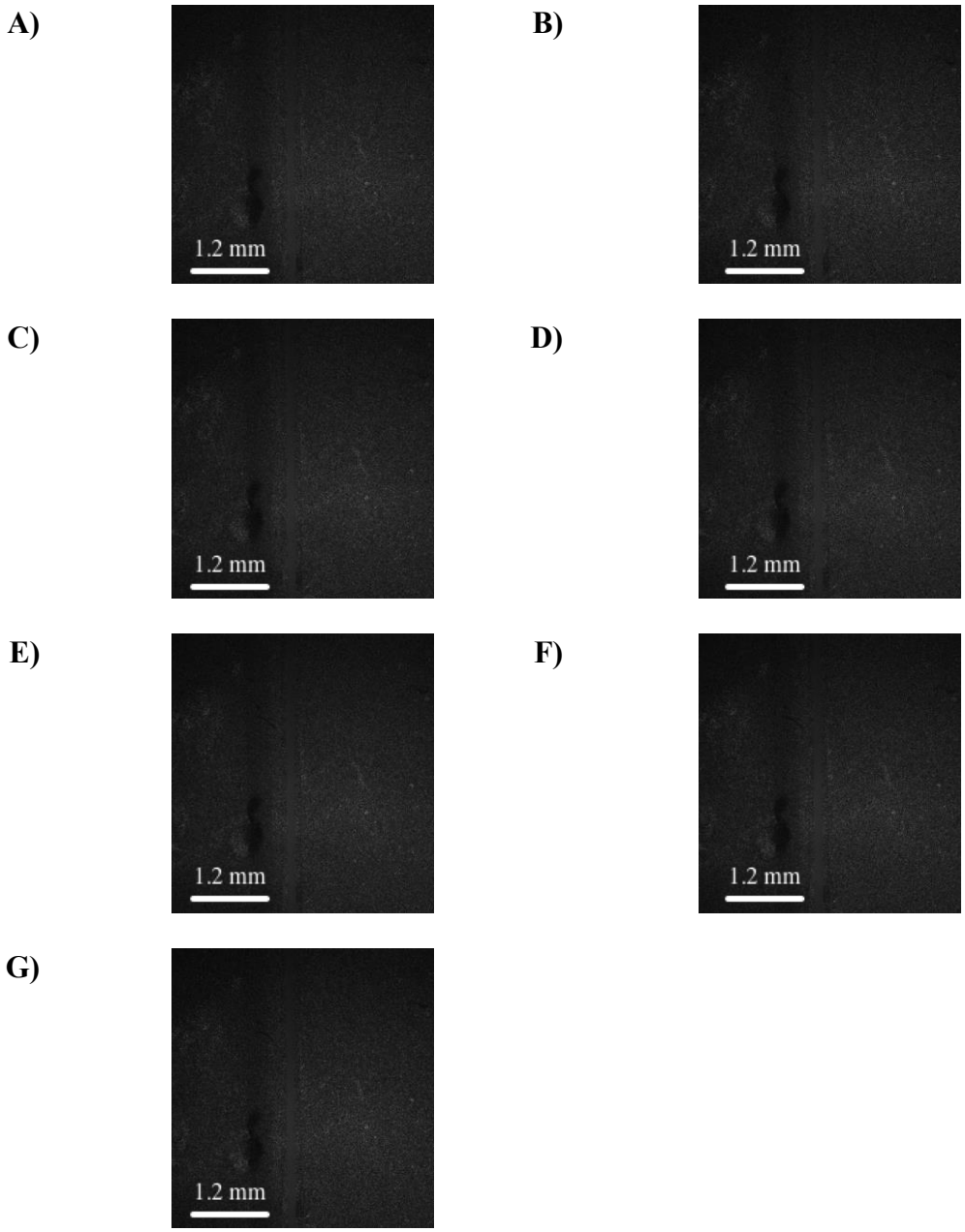

Figure 28 – Raw speckle images acquired by CCD camera for 2.0 mg/mL TiO_2 to PDMS background scattering. A) 1 mm/s flow B) 3 mm/s flow C) 5 mm/s flow D) 10 mm/s flow E) 15 mm/s flow F) 20mm/s flow G) 25 mm/s flow

Appendix D: Experimental Dynamic and Static Intensities

The following table contain the intensities measured from the dynamic medium and the accompanying static medium adjacent to it. This was done for all four experimental samples. As was discussed earlier, the dynamic intensity increased as the static background intensity increased. This fact is shown below in Table 6.

Table 6: Experimental Dynamic and Static Intensities

	TiO_2 Concentrations mg/mL			
Intensity	**0.0**	**0.5**	**1.0**	**2.0**
Static	2126	3637	4616	8225
Dynamic	4651	6893	8803	9859

Appendix E: Simulation Code

The following appendix section contains the code that was used to simulate speckle in this paper. If more information is desired regarding the function for speckle simulation please contact Dr. Duncan or Dr. Kirkpatrick. [8]

Dynamic Speckle Simulation

```
%creates expanded speckle patterns and averages them together to
simulate
%varying values of the ratio of decorrelation time to exposure time

[ogfram,~,~] = focal_plane_boil(252,4,1);
%frames = [25 76 127 151 202 253 756 1260 2520];
%frames = [12650 4216 3162 2530 1265 506 316 253];
frames = [4216 3162 2530 1264 508 316 252];
seed = 2;

for n = 1:30
 n
seed = seed + 1;

[cube,~,~] = focal_plane_boil(252,4,seed);
%cubenew(:,:,:,n) = cube(:,:,:);
    %for i = 1:50
    for i = 1:17
        i
        seed = seed + 1;

        [tempcube,~,~] = focal_plane_boil(252,4,seed);

        cube= cat(3,cube,tempcube);

    end
    %comp = bsxfun(@plus,cube,ogfram(:,:,1)/3);
    %cubestore(:,:,:,n) = comp(:,:,:);

    for g = 1:7
        tempmeancomp(:,:,n,g) = mean(comp(:,:,1:frames(g)),3);
%
    end

%  for z = 1:3
%  result = lasca(mean(cube(:,:,1:frames(z)),3),7);
%  means(z,n) = mean(result(:));
%  end
    %comp(:,:, = bsxfun(@plus,cube,ogfram(:,:,1));
```

```
end

% for g = 1:3
%     for b = 1:8
%         tempmean = cubestore(:,:,1:frames(z),g);
%         tempcube = mean(tempmean,3);
%         final(:,:,g,b) = tempcube;
%     end
% end
%
%
%  for d = 1:8
%  meow = final(:,:,:,d);
%  [dyn_trace, contrast_trace, ~,~] = dlsi_proc(meow, 7, 0);
%  means(d) = mean(dyn_trace(:));
%  end

%
%  for z = 1:8
%  [dyn_trace, contrast_trace, ~,~] =
dlsi_proc(mean(comp(:,:,1:frames(z),:),4), 7, 0);
%  means(z,n) = mean(dyn_trace(:))
%  end
```

Introducing the Static Contribution to the Dynamic Simulation

```
%Add a static speckle pattern the inputed dynamic patterns with varying
%intensities of the static pattern

c = [0 1/4 1/2 1 2 4 6 8 16 32];
ratio = c./(c+1);
for m = 1:10
for n = 1:30

    for g = 1:7

        tempcomp(:,:,n,g) =
bsxfun(@plus,tempmean(:,:,n,g),(c(m))*ogfram(:,:,1));

    end
end

for z = 1:7

   tem = tempcomp(:,:,:,z);
   [dyn_trace, contrast_trace, rho_trace,~] = dlsi_proc(tem, 7, 0);
   meansdyn(z,m) = mean(dyn_trace(:));
   meansstatic(z,m) = mean(rho_trace(:));
   meansmes(z,m) = mean(contrast_trace(:));
   kmav = sqrt(contrast_trace.^2 - beta*(rho_trace.^2));
```

```
    km(z,m) = abs(mean(kmav(:)));


end

%km = sqrt(meansmes.^2 - beta.*(meansstatic.^2)); %sqrt(meansmes.^2 -
0.988*meansstatic.^2);
end

dynavg = mean(meansdyn,1);
mesavg = mean(meansmes,1);
statavg = mean(meansstatic,1);
%end

%x = fliplr(253./[25 76 127 206 253 756 1260 2520]);

% figure(1)
%
%  semilogx(x,flipud(means),'ro')
%
%
% axis([10^-2 20 0 1])

figure(1)
subplot(1,3,1)
scatter(meansstatic(1,:),meansdyn(1,:),'k+')
hold on
scatter(meansstatic(2,:),meansdyn(2,:),'ko')
scatter(meansstatic(3,:),meansdyn(3,:),'k*')
scatter(meansstatic(4,:),meansdyn(4,:),'ks')
scatter(meansstatic(5,:),meansdyn(5,:),'kx')
scatter(meansstatic(6,:),meansdyn(6,:),'k^')
xlabel('rho estimation')
ylabel('K Dynamic')
set(gca,'fontsize',20)
set(findall(figure(1),'type','text'),'fontSize',20,'fontWeight','bold')
subplot(1,3,2)
scatter(meansstatic(1,:),km(1,:),'k+')
hold on
scatter(meansstatic(2,:),km(2,:),'ko')
scatter(meansstatic(3,:),km(3,:),'k*')
scatter(meansstatic(4,:),km(4,:),'ks')
scatter(meansstatic(5,:),km(5,:),'kx')
scatter(meansstatic(6,:),km(6,:),'k^')
xlabel('rho estimation')
ylabel('K12 Alternate')
set(gca,'fontsize',15)
subplot(1,3,3)
scatter(meansstatic(1,:),meansmes(1,:),'k+')
hold on
scatter(meansstatic(2,:),meansmes(2,:),'ko')
scatter(meansstatic(3,:),meansmes(3,:),'k*')
scatter(meansstatic(4,:),meansmes(4,:),'ks')
scatter(meansstatic(5,:),meansmes(5,:),'kx')
scatter(meansstatic(6,:),meansmes(6,:),'k^')
```

```
xlabel('rho estimation')
ylabel('K Measured')
legend('Tau/T = 0.08','Tau/T = 0.1','Tau/T = 0.2','Tau/T = 0.5','Tau/T
= 0.8','Tau/T = 1')
set(gca,'fontsize',20)
set(findall(figure(1),'type','text'),'fontSize',20,'fontWeight','bold')
```